

Engineering Hierarchical Symmetries

Zhanpeng Fu,^{1,2} Roderich Moessner,¹ Hongzheng Zhao,^{1,3,*} and Marin Bukov¹

¹*Max Planck Institute for the Physics of Complex Systems, Nöthnitzer Str. 38, 01187 Dresden, Germany*

²*Zhiyuan College, Shanghai Jiao Tong University, 200240, Shanghai China*

³*School of Physics, Peking University, 100871, Beijing China*

(Dated: February 22, 2024)

We present a general driving protocol for many-body systems to generate a sequence of prethermal regimes, each exhibiting a lower symmetry than the preceding one. We provide an explicit construction of effective Hamiltonians exhibiting these symmetries. This imprints emergent quasi-conservation laws hierarchically, enabling us to engineer the respective symmetries and concomitant orders in nonequilibrium matter. We provide explicit examples, including spatiotemporal and topological phenomena, as well as a spin chain realizing the symmetry ladder $SU(2) \rightarrow U(1) \rightarrow \mathbb{Z}_2 \rightarrow E$.

I. INTRODUCTION

Symmetry is ubiquitous in nature, and it underpins intriguing and fundamental phenomena including the existence of conservation laws, integrability, the classification of phases of matter and transitions between them [1, 2], and it is a crucial component of a plethora of topological phenomena [3, 4]. Therefore, exploring protocols to engineer a desired symmetry and control its breaking, as well as investigating emergent phenomena associated with engineered symmetries, has attracted long-standing interest in both fundamental physics [5–11] and quantum engineering [12–14].

Recently, time-dependent protocols were proposed to Floquet-engineer symmetry as an emergent phenomenon [15–21], leading to the discovery of nonequilibrium phases of matter [22–31]. However, little has been known about how to engineer sequences of different symmetries in a simple and controlled setting. This is a question of considerable importance for a variety of reasons. In statistical physics, symmetries can significantly impact how a system reaches thermal equilibrium [32–38]. Moreover, temporal sequences with specific symmetry content can be used to stabilize order in Floquet-engineered matter [39, 40]. They can also give rise to an interesting interplay of spontaneous with explicit symmetry breaking: from a practical perspective, engineered time-dependent symmetries can potentially enhance the control over wanted or unwanted spontaneous symmetry-breaking processes on real quantum devices [7, 41–48].

In this work we study the engineering of hierarchical symmetries (HS) in a time-dependent set-up: we investigate whether or not, and under which conditions, a sequence of emergent symmetries can be engineered to occur hierarchically in time, in a controllable way. Realizing such HS in time-dependent systems is a demanding challenge, since: (1) A priori, explicit symmetry-breaking processes do not in general preserve any subgroup structure, and introduce transitions among all possible symmetry sectors; (2) Due to the absence of energy conser-

vation in time-dependent systems, heating can further speed up the destruction of manifestations of symmetries, in particular quickly degrading any features sensitive to symmetry, e.g., melting any spontaneous-symmetry-breaking order.

Here, we propose a way to overcome these difficulties and construct a generic protocol to realize HS in driven many-body systems; it applies to any hierarchical symmetry group structure, irrespective of the specific microscopic details of the underlying model. It is explicit in that we provide a general scheme for realising any sequence of HS. In addition, this construction is not limited to Floquet systems, and also applies to more general time-dependence, e.g., quasi-periodically [28, 49–55], and even some randomly [56, 57], driven systems.

The key conceptual ingredient is a recursive time-dependent ansatz, in which unwanted processes, breaking a desired higher symmetry explicitly, cancel hierarchically in the high-frequency regime, cf. Fig. 1(a). Therefore, different symmetry-breaking effects only become noticeable beyond a sequence of long timescales. This leads to a corresponding sequence of prethermal steady-states with controllable lifetimes, each exhibiting a lower symmetry than the preceding one, cf. Fig 1(b) and (c) for an example. Our protocol thus also allows us to imprint emergent quasi-conservation laws hierarchically. Further, in conjunction with the process of spontaneous symmetry breaking, our scheme enables the engineering of different types of prethermal nonequilibrium order within the same time evolution.

Our account is structured as follows. We first present a definition of hierarchical symmetry, and discuss its realization using nonequilibrium drives in Sec. II. This establishes the conceptual framework and as a result identifies the central ingredients of a pair of protocols, one of which is of operational simplicity and efficiency, while the other is of complete generality. In Sec. III we lay out an intuitive picture of our central result, illustrated by three explicit applications: (i) a spin chain with three engineered distinct prethermal steady-states, characterized by continuous non-Abelian $SU(2)$, Abelian $U(1)$, and discrete \mathbb{Z}_2 symmetry, respectively; (ii) a quantum clock model featuring a dynamical crossover between prether-

* hzhao@pku.edu.cn

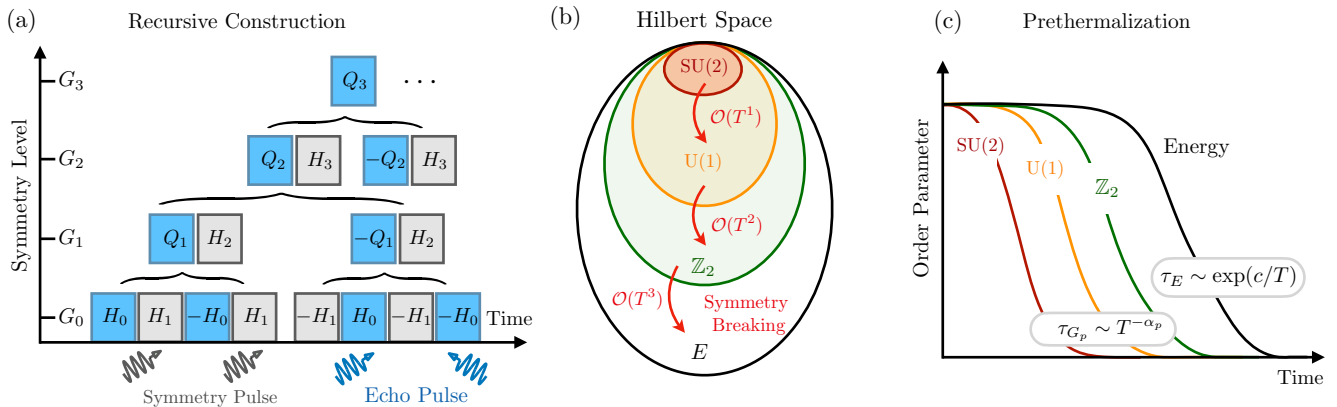


FIG. 1. (a) Hierarchical symmetry breaking can be engineered via a recursive construction, where the “symmetry pulse” imposes a higher symmetry structure while the “echo pulse” cancels unwanted symmetry-breaking processes order by order. (b) Hilbert space showing a paradigmatic example of the symmetry ladder $SU(2) \rightarrow U(1) \rightarrow \mathbb{Z}_2 \rightarrow E$, with E denoting the trivial group. Symmetry breaking process can be parametrically suppressed by using a smaller driving period T . (c) Schematic for the sequence of prethermal steady states, exhibiting a lower symmetry than the preceding one. Their lifetimes scale algebraically with T while heating in energy can be exponentially suppressed.

mal steady-states without equilibrium counterpart that exhibit \mathbb{Z}_4 and \mathbb{Z}_2 time crystalline order; and (iii) a free fermion system supporting a change in topology between a topological insulator (TI) and a higher-order topological insulator (HOTI) upon breaking time-reversal symmetry, as exemplified by the dynamical reduction of edge modes to corner/hinge modes in successive prethermal steady-states. We close with a summary of our results and an outlook with future applications in Sec. IV. Copious technical details are covered in supplemental materials.

II. IMPLEMENTING HIERARCHICAL SYMMETRIES

A. General recursive driving protocol

We first present our most fundamental result, namely an explicit general scheme for obtaining the HS for symmetry ladders as advertised above. We do this using the example of periodic drives, but the constructions proposed below are not limited to Floquet systems with step drives, and can also occur for continuous drives [58], and even quasi-periodically or randomly driven systems, as long as the dynamics can be approximated in a perturbative expansion by a sequence of effective Hamiltonian.

Consider a family of periodically driven systems, whose evolution operator over one period, U_F , is defined by concatenating l (different) time evolution operators:

$$U_F = U_l U_{l-1} \cdots U_1 \equiv e^{-iTQ}. \quad (1)$$

Whenever the drive frequency $\omega = 2\pi/T$ is large compared to the typical local energy scales, periodically (and even randomly) driven systems exhibit a long-lived

prethermal plateau [28, 56, 59–61] as a result of energy quasi-conservation. The dynamics can be approximated by a static effective Hamiltonian $Q_{[M]}$, obtained by means of the inverse-frequency expansion (IFE) [59]:

$$Q_{[M]} = \sum_{m=0}^M Q^{(m)}, \quad Q^{(m)} \propto T^m, \quad (2)$$

with M denoting the truncation order. Hence, generic ergodic systems evolve into a prethermal metastable state, described by the Generalized Canonical Ensemble, $\hat{\rho}_{\text{GCE}} \sim \exp(-\sum_{\alpha} \lambda_{\alpha} C_{\alpha})$, with conserved quantities C_{α} associated with $Q_{[M]}$, and the Lagrange multipliers $\{\lambda_{\alpha}\}$ fixed by the initial state [10, 33]. We aim to construct a generic protocol that inscribes a structure of hierarchical symmetries into $Q_{[M]}$, one corresponding to each order $Q^{(m)}$ of the IFE. If we start from an ordered initial state that breaks the highest symmetry in $Q^{(0)}$, these symmetries will be revealed in the dynamics of the system via the occurrence of a hierarchical series of prethermal plateaus, cf. Fig 1(c).

Concretely, consider a finite set of Hamiltonian generators H_n, H_{n-1}, \dots, H_0 and an associated ladder of symmetry groups $G_n \supset G_{n-1} \supset \cdots \supset G_0$. Each Hamiltonian H_p preserves the corresponding symmetry group G_p , so that $[H_p, S_q] = 0$ for all generators S_q of G_q with $q \leq p$; equivalently, each Hamiltonian H_p breaks only one subsymmetry of the symmetry ladder, reducing the symmetry group G_{p+1} to G_p .

We realize such a symmetry hierarchy dynamically, by imprinting it iteratively in the structure of the effective Hamiltonian (2), order by order in the IFE. The Floquet unitary at (hierarchy) level- n is constructed recursively as

$$U_{F,n} = e^{-il_{n-1}TQ_{n-1}} e^{-iT H_n} e^{+il_{n-1}TQ_{n-1}} e^{-iT H_n} \quad (3)$$

where $l_n = 3 \times 2^n - 2$ is the length of drive sequence, and we set $Q_0 = H_0$, cf. Fig. 1(a). The effective stroboscopic generator at level- n is defined via the relation, $U_{F,n} \equiv e^{-i l_n T Q_n}$ [62]. In A, we prove by induction that the corresponding IFE approximation at order m , $Q_n^{(m)} \propto T^m$ [cf. Eq. (2)], preserves the symmetry group G_{n-m} , ($n-m \geq 0$), and breaks explicitly all higher symmetries up the ladder. The key ingredient of this construction is that, in Eq. (3), the prefactors in front of the two Q_{n-1} operators differ by a sign, ensuring the exact cancellation of G_n symmetry-breaking terms in the leading order (time-average) $Q_n^{(0)}$.

B. Illustration of HS for small n

Let us explicitly illustrate the mechanism behind HS using a concrete example for small n . For $n=1$, we have

$$U_{F,1} = e^{-i H_0 T} e^{-i H_1 T} e^{i H_0 T} e^{-i H_1 T}. \quad (4)$$

The effective Hamiltonian to leading orders consists of $Q_1^{(0)} \sim H_1$ which preserves G_1 , and $Q_1^{(1)} \sim T[H_1, H_0]$ which reduces G_1 to G_0 . Notice that the opposite signs in the prefactors in front of the two H_0 generators in the drive sequence ensure the exact cancellation of the G_1 -breaking terms H_1 in the leading order $Q_1^{(0)}$; they only become effective at $\mathcal{O}(T)$ in $Q_1^{(1)}$.

At hierarchy level $n=2$, we introduce a new Hamiltonian H_2 which preserves G_2 (and hence also its subgroups G_1 and G_0). The new time evolution operator is $U_{F,2} = e^{-i Q_1 l_1 T} e^{-i H_2 T} e^{i Q_1 l_1 T} e^{-i H_2 T}$. Now $Q_2^{(0)} \sim H_2$ preserves G_2 , while $Q_2^{(1)} \sim T[H_2, H_1]$ reduces G_2 to G_1 ; finally, $Q_2^{(2)}$ contains a term $T^2[H_2, [H_1, H_0]]$ which explicitly breaks G_1 to G_0 . Note that, in practice, $e^{i Q_1 l_1 T}$ can be implemented by reversing the order of the temporal sequence of Eq. (4) and conjugating each individual driving element (i.e., going backward in time); this operation is generally accessible on current quantum computing platforms [31].

This construction can be performed recursively for higher n and, remarkably, for each successive order of the IFE of the HS protocol in Eq. (3), $Q_n^{(m)}$ breaks only the corresponding successive subgroup, as desired. Note that we do not make any assumptions about the microscopic details of the generators H_n ; hence, our construction is completely general and applies to any hierarchical symmetry group structure, making it widely applicable.

C. Sequence length, and shortening

Due to its recursive character, the generic driving sequence (3) is exponentially long, $l_n \sim 2^n$, in the number n of elementary unitary operators of the form $\exp(-i c H_k)$. Its appeal lies in its complete generality. Naturally, when considering applications to real physical systems

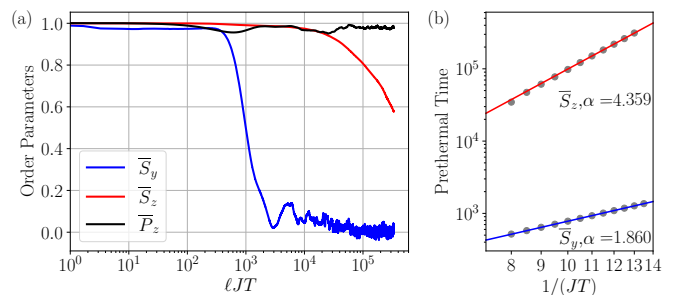


FIG. 2. Dynamical detection of $SU(2) \rightarrow U(1) \rightarrow \mathbb{Z}_2 \rightarrow E$ HS. (a) Dynamics of order parameters for the hierarchical quasi-conservation laws. Observables are normalized w.r.t. their initial values such that they all start from unity. Different lifetimes suggest that HS emerge at different time scales. (b) Lifetimes for each quasi-conservation law can be prolonged parametrically as $T^{-\alpha}$ in the high-frequency limit. The scaling exponent α follows the prediction by Fermi's Golden Rule. We use $\delta_x/J=10$, $\epsilon/J=6$ and the coupling strength $J'/J=5$. The numerical simulations are performed using exact diagonalization and 30 random realizations of the driving protocol and initial state are used to compute the ensemble average.

(Sec. III), it is worthwhile to consider ways to shorten this sequence. Indeed, one can anticipate that the algebraic structure of the drive Hamiltonians may allow further contractions of the protocol.

As a concrete illustration of this possibility, consider three Hamiltonians $H_{2,1,0}$ corresponding to $G_2 \supset G_1 \supset G_0$; if, in addition, they obey the relation $[H_0, H_1 + H_2] = 0$, then the shorter protocol

$$U_F = (e^{-i H_0 T} e^{-i H_1 T}) e^{-i H_2 T} (e^{i H_0 T} e^{i H_1 T}) e^{-i H_2 T} = e^{-i T Q} \quad (5)$$

defines an effective Hamiltonian, such that $Q_2^{(0)} = H_2$ has the symmetry group G_2 , $Q_2^{(1)}$ reduces G_2 to G_1 , and $Q_2^{(2)}$ breaks explicitly G_1 to G_0 . A simple realization in spin-1/2 chains, discussed in C, corresponds to the symmetry ladder $U(1) \rightarrow \mathbb{Z}_2 \rightarrow E$, with $E = \{id\}$ the trivial group. In the next section, we use this idea to implement an even more exotic four-step HS protocol featuring a non-abelian symmetry.

III. APPLICATIONS

In this section, we present applications of hierarchically engineered symmetries for three very different concepts/phenomena – non-Abelian symmetry, spatiotemporal order, and topological properties.

A. Implementation of Hierarchical Abelian and non-Abelian Symmetries

We uncover the effects of HS via numerically simulating the dynamics of a paradigmatic many-body spin

system with a rich emergent hierarchical symmetry structure $SU(2) \rightarrow U(1) \rightarrow \mathbb{Z}_2 \rightarrow E$. To demonstrate that HS can occur beyond time-periodic systems, we consider a system driven by a fully random sequence built out of two possible unitaries U_{\pm} :

$$U_{\pm} = U(-H_0^{\pm}, H_1, H_2, H_0^{\pm}, -H_1, H_2, H_3|T/14) \times \quad (6)$$

$$U(-H_2, H_1, -H_0^{\pm}, -H_2, -H_1, H_0^{\pm}, H_3|T/14),$$

where we define $U(D_1, \dots, D_l|T) = e^{-iD_1 T} \dots e^{-iD_l T}$ for simplicity, with many-body spin-1/2 generators

$$H_3 = J \sum_{\langle i,j \rangle} \sigma_i^x \sigma_j^x + \sigma_i^y \sigma_j^y + \sigma_i^z \sigma_j^z,$$

$$H_2 = J' \sum_{\langle i,j \rangle} \sigma_i^x \sigma_j^x + \sigma_i^y \sigma_j^y - \sigma_i^z \sigma_j^z, \quad (7)$$

$$H_1 = -J' \sum_{\langle i,j \rangle} \sigma_i^y \sigma_j^y - \sigma_i^z \sigma_j^z,$$

$$H_0^{\pm} = (\delta_x \pm \epsilon) \sum_i \sigma_i^x.$$

The spins interact with their nearest neighbors with strength J and J' , and a uniform x -field of amplitude $\delta_x \pm \epsilon$ is applied randomly in time as the protocol sequence grows.

One can derive two different effective Hamiltonians Q_{\pm} for U_{\pm} , which coincide up to the order $\mathcal{O}(T^2)$, $Q_{+}^{(m)} = Q_{-}^{(m)}$ for $m=0, 1, 2$; this happens since, in the driving protocol, the only difference occurs through H_0^{\pm} , whose effect is suppressed to order $m \leq 2$ by the special construction Eq. (6). To leading order, summing up all generators, it is easy to see that $Q_{\pm}^{(0)} \propto H_3$ reproduces the Heisenberg model, preserving the highest symmetry $SU(2)$; moreover, using IFE and the property $[H_0^{\pm}, H_1 + H_2] = 0$, one can show that $Q_{\pm}^{(1)} = \mathcal{O}(T)$ reduces $SU(2)$ to $U(1)$; in turn, $Q_{\pm}^{(2)} = \mathcal{O}(T^2)$ further reduces $U(1)$ to a \mathbb{Z}_2 symmetry generated by the parity operator $P_z = \prod_i \sigma_i^z$ [63], cf. Fig 1(b) and C. This \mathbb{Z}_2 symmetry itself is weakly but explicitly broken by higher-order terms. Consequently, it is expected that, if we start from an $SU(2)$ -broken initial state, the quasi-conservation laws associated with the above symmetries will persist with different lifetimes in the high-frequency (or small T) regime.

To verify this, we first prepare the initial state $|\psi(0)\rangle$ as a Haar random state in the z -magnetization block containing $N_{\downarrow}=6$ down spins out of all $L=16$ sites; it is then rotated around the x -axis by $\prod_i e^{-i\pi/16\sigma_i^x}$, resulting in an ordered state with non-zero initial magnetization along the z and y directions [64]. If the $SU(2)$ symmetry is preserved, both $S_y = \sum_i \sigma_i^y$ and $S_z = \sum_i \sigma_i^z$ are quasi-conserved quantities. As illustrated in Fig. 2a, for a fixed period $JT=0.1$, their normalized expectation values, $\bar{S}_{y/z}(t) = \langle \psi(t) | S_{y/z} | \psi(t) \rangle / \langle \psi(0) | S_{y/z} | \psi(0) \rangle$, indeed remain almost unchanged until a long time scale $J\ell T \approx 5 \times 10^2$. Then, the system exhibits a noticeable

decay in \bar{S}_x , indicating the explicit breaking of $SU(2)$ by the higher-order terms in the IFE. By contrast, the quasi-conservation of \bar{S}_z corresponding to the $U(1)$ symmetry is more robust, and only exhibits roughly 20% deviation from the initial unit value around $J\ell T \approx 5 \times 10^4$, when the y -magnetization completely vanishes.

To detect the preservation of the \mathbb{Z}_2 symmetry, we measure the normalized expectation value of the parity operator $\bar{P}_z(t)$ which remains close to its initial value throughout the entire time evolution that we can numerically simulate.

The dynamics, constrained by all of these emergent symmetries, can be stabilized by using a higher drive frequency, and consequently, the lifetime of each quasi-conservation law can be parametrically prolonged. We define the lifetimes τ_y and τ_z as the time when the magnetizations $\langle S_y(t) \rangle$ and $\langle S_z(t) \rangle$ drop below the threshold values e^{-1} and $e^{-0.45}$, respectively [65]. As shown in Fig. 2b, in the high-frequency limit, both time scales follow an algebraic scaling in the form of $\tau \sim T^{-\alpha}$ with the scaling exponent $\alpha \approx 2$ for \bar{S}_y , and $\alpha \approx 4$ for \bar{S}_z , following the Fermi's Golden Rule (FGR) prediction, cf. B. Since the \mathbb{Z}_2 -breaking perturbations of $\mathcal{O}(T^3)$ are extremely weak, it is challenging to determine the concrete scaling law for the lifetime of \bar{P}_z . In C, we consider another HS example to illustrate a simpler hierarchy $U(1) \rightarrow \mathbb{Z}_2 \rightarrow E$, where we show that the decay of \bar{P}_z can also be suppressed by using a shorter driving period. However, since \bar{P}_z is a non-local operator, its decay may not be described by FGR.

HS stabilize quasi-conservation laws for both Abelian and non-Abelian, continuous and discrete symmetries with the corresponding timescales parametrically under control. In the following, we will go beyond and demonstrate how HS can be harnessed to engineer different types of non-equilibrium order, connected by dynamical crossover regimes and corresponding to the hierarchical symmetry groups, including spatiotemporal order (STO) and higher order topological insulating states.

B. Hierarchical Symmetry Reduction in a \mathbb{Z}_4 Discrete Time Crystal

We begin with STO and consider a 4-state clock model, whose kicked dynamics is generated by

$$H_0 = \sum_{i=1}^L b_i (Z_i + Z_i^{\dagger})$$

$$H_1 = \sum_{\langle i,j \rangle} J_{ij} \left(Z_i^2 Z_j^2 - \eta (e^{i\phi} Z_i^{\dagger} Z_j + \text{h.c.}) \right) \quad (8)$$

$$+ \sum_i h_i \left(Z_i^2 - \frac{1}{2} (X_i + X_i^{\dagger}) \right) + \sum_i g_i X_i^2,$$

where J_{ij} is a nearest neighbor interaction strength, g_i an onsite X^2 interaction, and b_i is a parallel field; h_i

measures the strength of a combination of the onsite Z^2 -interaction and the transverse field; η and ϕ help stabilize the STO [66]. We introduce randomness in the form of uniformly distributed spatial disorder in all couplings, to reduce finite-size effects that manifest as temporal fluctuations in the dynamics of observables. In the Z -eigenbasis denoted by $|n\rangle$, $n = 0, 1, 2, 3$,

$$Z = \begin{pmatrix} 1 & 0 & 0 & 0 \\ 0 & -i & 0 & 0 \\ 0 & 0 & -1 & 0 \\ 0 & 0 & 0 & i \end{pmatrix}, \quad X = \begin{pmatrix} 0 & 1 & 0 & 0 \\ 0 & 0 & 1 & 0 \\ 0 & 0 & 0 & 1 \\ 1 & 0 & 0 & 0 \end{pmatrix}, \quad (9)$$

satisfy the commutation relations $Z_j X_k = e^{\frac{i\pi}{2}\delta_{jk}} X_k Z_j$, and $X_j^4 = 1 = Z_j^4$. The X operator shifts the population of the four $|n\rangle$ states cyclically. Hence, the internal level structure admits a \mathbb{Z}_4 symmetry. This symmetry is obeyed by the nearest-neighbor interaction and the X^2 terms, and broken down to a \mathbb{Z}_2 subgroup by the Z^2 onsite term; the parallel field further reduces this remaining symmetry to the trivial group, $\mathbb{Z}_2 \rightarrow E$.

When the kicked dynamics of the system, generated by H_0 and H_1 , is interleaved with T -periodic X -kicks, $P_X = \prod_i X_i$,

$$U_F = e^{iH_0 T/4} e^{-iH_1 T/4} e^{-iH_0 T/4} e^{-iH_1 T/4} P_X, \quad (10)$$

the \mathbb{Z}_4 symmetry can conspire with the discrete time-translation symmetry and induce spatiotemporal order, much like in a \mathbb{Z}_4 -time crystal [66]. The kick generators H_0, H_1 are designed to imprint HS in the first few orders of the effective Hamiltonian associated with Eq. (10). In particular, using the relation $\sum_{q=0}^3 [X^q]^\dagger Z^p X^q = 0$ ($p \in \mathbb{N}$), one can show that the leading-order term $Q^{(0)}$ has a \mathbb{Z}_4 symmetry which gets reduced to its \mathbb{Z}_2 subgroup by $Q^{(1)}$, while higher-order terms possess no symmetry; the explicit form of the effective Hamiltonian is given in D. As a result, the system exhibits two prethermal STO states within its time evolution (one for each emergent symmetry in the ladder), connected by a smooth crossover in time and stabilized by disorder.

Figure 3a shows the dynamics of the population $p^{(n)} = |n\rangle\langle n|$ of each of the four clock states $|n\rangle$ at times $t_\ell = 4\ell T$, averaged over the lattice, starting from the initial product state $|\psi(0)\rangle = |3\rangle^{\otimes L}$. Two prethermal plateaus, corresponding to \mathbb{Z}_4 and \mathbb{Z}_2 quasi-conservation, are clearly visible in Fig. 3a. Their lifetime can be increased by decreasing the drive period T . In the \mathbb{Z}_4 -plateau governed by $Q^{(0)}$, the population exhibits period-4 oscillations in time [Fig. 3b], characteristic of prethermal 4-DTC order. As time progresses, $Q^{(1)}$ asserts itself, and hence the dynamics crosses over to the \mathbb{Z}_2 -plateau. The explicit breakdown of the original \mathbb{Z}_4 -symmetry causes the population to redistribute, while subject to the surviving \mathbb{Z}_2 -quasi-constraint. As a result, akin to prethermal 2-DTC order, the population keeps oscillating between two states [Fig. 3c], described by a statistical mixture of the bare even/odd clock states that

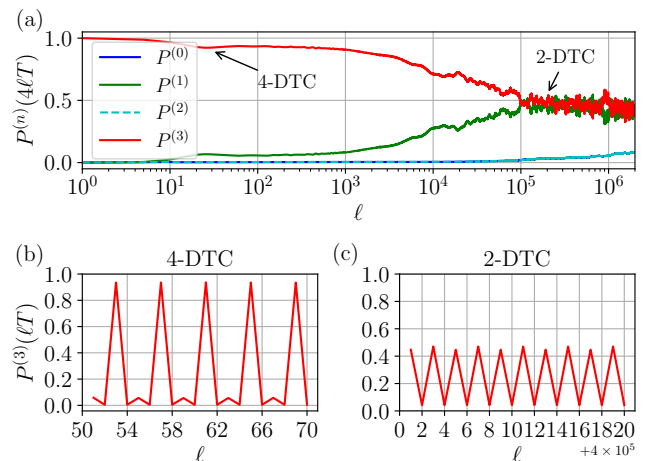


FIG. 3. \mathbb{Z}_4 quantum clock model. Time evolution of average population $P^{(n)}(t_\ell) = L^{-1} \sum_{j=1}^L \langle \psi(t_\ell) | p_j^{(n)} | \psi(t_\ell) \rangle$ in the clock state $|n\rangle$ at $t_\ell = 4\ell T$, starting from the initial state $|\psi(0)\rangle = |3\rangle^{\otimes L}$ and being averaged over 50 realizations. (a) Population $P^{(n)}(t_\ell)$ at $t_\ell = 4\ell T$ and the dynamic crossover between two spatial-temporal orders. (b) \mathbb{Z}_4 plateau, system oscillates between these four local state and their superposition which is a 4-DTC behaviour. (c) \mathbb{Z}_2 plateau, the odd and even local states merge in pairs (dash line), and system finally exhibit 2-DTC behavior. The parameters are $T = 0.5$, $\eta=0.35$, $\phi=\pi/3$, and $J_{ij} \in (0.5, 1.5)$, $g_i \in (0, 0.3)$, $h_i \in (0, 0.6)$, $b_i \in (0, 2.5)$ are drawn from a uniform distribution in the given interval.

halves the oscillation amplitude. Hence, the manifestation of this spatiotemporal HS ladder is reflected in the change of the characteristic periodic signature of observable expectations as a function of time. Due to the ultimate breakdown of the \mathbb{Z}_2 symmetry by the higher-order effective Hamiltonians $Q^{(m \geq 2)}$, the population gradually spreads over all clock states, as evidenced by the rise of the blue and cyan curves in Fig. 3a. Eventually, at even longer times the final state of the system is evenly distributed among the four clock states, corresponding to a featureless infinite-temperature state [not shown].

C. High-order Topological Insulators from Hierarchical Symmetries

Symmetries play a fundamental role also in topological quantum matter; this is perhaps most prominently encoded in the notion of symmetry-protected topological phases (SPTs), where topological stability is predicated on the presence of a particular symmetry [3, 4]. We now demonstrate how HS can change the topological character of, say, electronic systems by altering the underlying symmetry. We start from a topological insulator (TI) in a 2D lattice, protected by time reversal symmetry \mathcal{T} and crystalline inversion symmetry \mathcal{I} . Subject to open boundary conditions, the single-particle spectrum

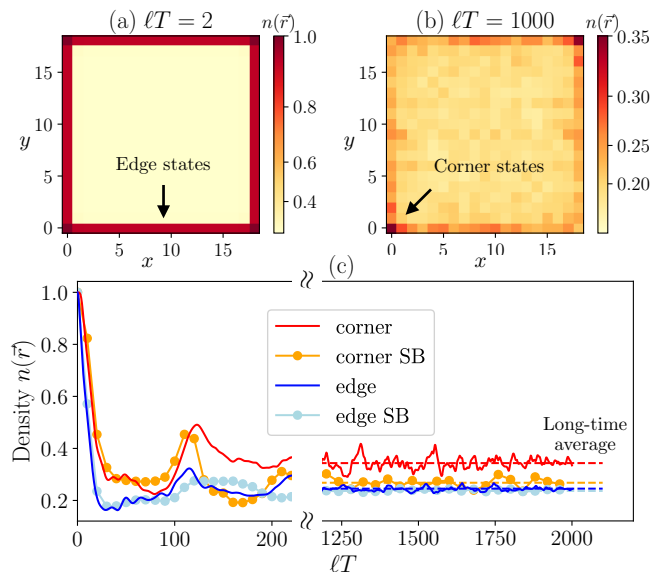


FIG. 4. **Topological corner states stabilized by HS.** Time evolution of the electron density on site $\vec{r} = (x, y)$, $n(\vec{r}) = \sum_{\sigma=\uparrow,\downarrow} \sum_{q=0,1} \langle c_{\sigma,q}^\dagger(\vec{r}) c_{\sigma,q}(\vec{r}) \rangle$, starting from the initial state that fully cover the edge. (a-b) Snapshots of the density distribution show a dynamical change of topology, manifest in a transition from an edge state (TI) to a corner state (HOTI). (c) Dynamics of the density at the corner (red line) $n_{\text{corner}} = (n(0,0) + n(L,L))/2$ and the edge (blue line) $n_{\text{edge}} = 2 \sum_{i=L/4}^{3L/4} n(i,0)/L$ using a HS ladder. If the first-order perturbation explicitly breaks \mathcal{I} , support on the corner becomes less dominant (orange) while the edge maintains approximately the same density at long times (dashed lines). We use $M = 1.0, J = 1.0, \Delta_0 = 1.0, \Delta_1 = 7.0, \Delta_2 = 12.0$ and $T = 0.2$ for numerical simulation.

of the Hamiltonian H_{TI} exhibits topological edge modes. In such materials, an initial state with significant support on the edge of a sample will keep this support during the time evolution generated by H_{TI} . Perturbations that break time reversal \mathcal{T} but preserve inversion symmetry \mathcal{I} cause a topological phase transition from a TI to a higher-order topological insulator (HOTI) [67]. The characteristic feature of HOTI is the presence of corner states whose support is localized only at the corners of the sample, reflecting the reduced symmetry group.

A change of topology from a TI to a HOTI can naturally be exhibited by the transient dynamics of Floquet systems that realize the HS ladder $\mathcal{T} \times \mathcal{I} \rightarrow \mathcal{I} \rightarrow E$. Intuitively, initial states with weight concentrated on the edge modes will remain stable over a controllable timescale, before the leading-order symmetry-reducing term takes over; then only modes supported on the corners survive, while other edge modes start delocalizing into the bulk as a result of broken time reversal. Eventually, if present, interactions will cause the system to heat up to an infinite temperature state and lose all nontrivial topological properties.

To demonstrate this explicitly, we consider the Floquet

unitary

$$U_F = U \left(H_0, \frac{H_1}{2}, \frac{H'_1}{2}, -H_0, \frac{H_1}{2}, \frac{H'_1}{2}, H_2 \left| \frac{T}{10} \right. \right) \times \quad (11)$$

$$U \left(-\frac{H_1}{2}, -\frac{H'_1}{2}, H_0, -\frac{H_1}{2}, -\frac{H'_1}{2}, -H_0, H_2 \left| \frac{T}{10} \right. \right)$$

for a set of four 4-band Hamiltonians $H_{0,1,2}^{(\prime)}$ on a 2D square lattice, involving two orbital angular momentum and two spin degrees of freedom, described by the Pauli matrices τ and σ , respectively. Going to momentum space using $H_j = \sum_{\vec{k}} \psi_{\vec{k}}^\dagger H_j(\vec{k}) \psi_{\vec{k}}$ with $\psi_{\vec{k}} = [c_{\uparrow,0}(\vec{k}), c_{\downarrow,0}(\vec{k}), c_{\uparrow,1}(\vec{k}), c_{\downarrow,1}(\vec{k})]$, we have

$$H_2(\vec{k}) = [M + J(\cos k_x + \cos k_y)] \tau_z \sigma_0$$

$$H_1(\vec{k}) = \Delta_1 \tau_z (\sigma_x + \sigma_y),$$

$$H'_1(\vec{k}) = \Delta_1 \tau_z \sigma_z,$$

$$H_0(\vec{k}) = \Delta_2 \tau_x \sigma_y. \quad (12)$$

The representation of the Hamiltonian in real space is shown in D. Compared to Eq. (3), Eq. (11) features additionally H'_1 which introduces an onsite \mathcal{T} breaking term in the effective Hamiltonian that opens up the energy gap at the band touching point of H_2 to produce the HOTI.

The time-reversal symmetry can be represented as $\mathcal{T} = i\tau_0 \sigma_y K$, with K the complex conjugation, and acts on the Hamiltonian (12) by $\vec{k} \rightarrow -\vec{k}$ and $\mathcal{T} \vec{\sigma} \mathcal{T}^{-1} = -\vec{\sigma}$; inversion symmetry $\mathcal{I} = \tau_z \sigma_0$ transforms $\vec{k} \rightarrow -\vec{k}$ and $\mathcal{I} \tau_{x,y} \mathcal{I}^{-1} = -\tau_{x,y}$. Therefore, H_2 is invariant under both \mathcal{I} and \mathcal{T} , and hosts the well-known \mathbb{Z}_2 -TI for $|M| < 2|J|$. As a consequence, the leading order effective Hamiltonian $Q^{(0)} \propto H_2$ inherits the topological property of H_2 . Moreover, note that the terms proportional to Δ_1 break \mathcal{T} , while the Δ_2 term breaks both \mathcal{T} and \mathcal{I} ; therefore, $Q^{(1)} \propto \tau_0 (\sigma_x - \sigma_y)$ breaks \mathcal{T} but preserves \mathcal{I} . This allows the protocol in Eq. (11) to induce a dynamical crossover in topological order from TI to HOTI. The complete effective Hamiltonian and its eigenvalue spectrum can be found in D.

To exhibit this topological HS ladder, we prepare the initial state as the product state in the real-space Fock basis to fully cover the edge of the 2D lattice; on each edge site the same internal degree of freedom ($\downarrow, 1$) is occupied, i.e., $|\psi_0\rangle = \prod_{\vec{r} \in \text{edge}} c_{\downarrow,1}^\dagger(\vec{r}) |0\rangle$. Since this initial state has a large overlap with the localized edge state of $Q^{(0)}$, the initial configuration remains almost unchanged at the early evolution times, as shown by the real-space density $n(\vec{r})$ at time $\ell T = 2$ in Fig. 8a. The persistence of the edge density can be more pronounced if we initialize the system in one of the localized eigenstates of $Q^{(0)}$, cf. E.

At later times, the system starts delocalizing into the bulk but the occupation around the corners persists, cf. Fig. 8b, due to the surviving inversion symmetry in $Q^{(1)}$, which is required for the HOTI [in our model, the zero-energy corner state occupies only two of the four

corners]. We also depict the density at the corner (red line) and the edge (blue line) in panel Fig. 8c; clearly, the corner density has larger support especially at long times (dashed lines).

To highlight the importance of using HS in stabilizing the corner state, we also plot the dynamics (dotted lines) with different Hamiltonians $H_1 = \Delta_1 \tau_x (\sigma_x + \sigma_y)$, $H'_1 = \Delta_1 \tau_0 \sigma_z$, such that the first order IFE correction explicitly breaks all symmetries at once. As shown in panel Fig. 8c, in this case, the support on the corner state (dotted orange) stabilizes at twice a smaller value compared to the HS case [68]. By contrast, the edge density (light blue) remains approximately unchanged at long times.

IV. DISCUSSION AND OUTLOOK

We present a constructive framework to engineer symmetry reduction hierarchically in driven many-body systems via a recursive time-dependent ansatz. This permits us to impose hierarchical quasi-conservation laws and to realize various kinds of order in nonequilibrium matter. The lifetime of such ordered states accessible via HS, is parametrically controllable and can be obtained using Fermi's Golden rule, see B.

We demonstrate HS in systems with different global symmetries, inducing dynamical crossovers between both equilibrium and nonequilibrium ordered states, including topological states. The generalization to local gauge symmetries presents an interesting open direction [69]: e.g., in the Floquet-engineered Kitaev honeycomb model [19–21] HS can play an important role in stabilizing exotic fractionalized phases of matter. HS also have the potential to significantly suppress errors in the quantum simulation of time-dependent systems thereby improving the robustness of quantum algorithms whenever symmetry plays a central role as in, e.g., quantum error correction [70–72].

HS constructions apply equally to fermionic and bosonic, interacting and noninteracting quantum models that exhibit hierarchical symmetries and are, therefore, widely accessible in various experimental platforms. For example, the Heisenberg model with tunable anisotropy in Eq. (8) has already been realized in cold atoms systems and superconducting qubits [14, 47, 73, 74]. HS can be readily implemented in the lab since the underlying echo-out mechanism generalizes state-of-the-art dynamical decoupling techniques [44]; they can also be used to

achieve enhanced control over higher-order corrections. Particularly intriguing is the possibility of experimentally studying the properties of distinct ordered states within different prethermal stages of the same time evolution.

On a fundamental level, spontaneous symmetry breaking (SSB) of *approximate* (i.e., weakly explicitly broken) continuous symmetries gives rise to weakly *gapped* Goldstone modes [75]. These gapped excitations will naturally appear during the hierarchical symmetry breaking of $SU(2) \rightarrow U(1) \rightarrow \mathbb{Z}_2 \rightarrow E$, provided that the system is initialized at low-enough temperatures. A systematic investigation of this phenomenon would provide valuable insights on SSB in driven systems, opening up new avenues for future work.

We emphasize that discussions regarding engineered symmetry breaking are not limited to quantum or Hamiltonian systems. It is intriguing to generalize the analysis of the symmetry structure to Liouvillians [76–79], and we anticipate applications of HS in time-dependent open quantum systems and classical many-body setups. In particular, numerical simulation of classical systems is not limited to small system sizes and hence novel prethermal phases in higher dimensions induced by HS can be explored [80–84]. Understanding the richer hierarchical structure of weak and strong symmetries in open systems is an open avenue for future studies [71, 85]. Moreover, generalizing the current framework to engineer integrability breaking [86] and to control classical chaos would be worthwhile to pursue.

Finally, our work also raises the intriguing converse question of whether or not one can design protocols that systematically enlarge a given symmetry group.

Acknowledgments.—We thank A. Dymarsky, M. Heyl, F. Pollmann, F. Schindler and Y. Hou for enlightening discussions. This work is in part supported by the Deutsche Forschungsgemeinschaft under cluster of excellence ct.qmat (EXC 2147, project-id 390858490). Funded by the European Union (ERC, QuSimCtrl, 101113633). Views and opinions expressed are however those of the authors only and do not necessarily reflect those of the European Union or the European Research Council Executive Agency. Neither the European Union nor the granting authority can be held responsible for them. This research was supported in part by the International Centre for Theoretical Sciences (ICTS) for participating in the program - Stability of Quantum Matter in and out of Equilibrium at Various Scales (code: ICTS/SQMVS2024/01)

-
- [1] L. D. Landau and E. M. Lifshitz, *Statistical Physics: Volume 5*, Vol. 5 (Elsevier, 2013).
 - [2] P. M. Chaikin, T. C. Lubensky, and T. A. Witten, *Principles of condensed matter physics*, Vol. 10 (Cambridge university press Cambridge, 1995).
 - [3] F. Pollmann, E. Berg, A. M. Turner, and M. Oshikawa, Symmetry protection of topological phases in

one-dimensional quantum spin systems, *Physical review b* **85**, 075125 (2012).

- [4] X. Chen, Z.-C. Gu, Z.-X. Liu, and X.-G. Wen, Symmetry protected topological orders and the group cohomology of their symmetry group, *Physical Review B* **87**, 155114 (2013).
- [5] P. W. Anderson, An approximate quantum theory of the

- antiferromagnetic ground state, *Physical Review* **86**, 694 (1952).
- [6] M. Dine, W. Fischler, and M. Srednicki, A simple solution to the strong cp problem with a harmless axion, *Physics letters B* **104**, 199 (1981).
- [7] T. Brauner, Spontaneous symmetry breaking and nambu–goldstone bosons in quantum many-body systems, *Symmetry* **2**, 609 (2010).
- [8] C. Castelnovo, R. Moessner, and S. L. Sondhi, Spin ice, fractionalization, and topological order, *Annu. Rev. Condens. Matter Phys.* **3**, 35 (2012).
- [9] D. A. Abanin, W. De Roeck, and F. Huveneers, Exponentially slow heating in periodically driven many-body systems, *Physical review letters* **115**, 256803 (2015).
- [10] T. Kuwahara, T. Mori, and K. Saito, Floquet–magnus theory and generic transient dynamics in periodically driven many-body quantum systems, *Annals of Physics* **367**, 96 (2016).
- [11] B. Bertini, F. Heidrich-Meisner, C. Karrasch, T. Prosen, R. Steinigeweg, and M. Žnidarič, Finite-temperature transport in one-dimensional quantum lattice models, *Reviews of Modern Physics* **93**, 025003 (2021).
- [12] E. A. Martinez, C. A. Muschik, P. Schindler, D. Nigg, A. Erhard, M. Heyl, P. Hauke, M. Dalmonte, T. Monz, P. Zoller, *et al.*, Real-time dynamics of lattice gauge theories with a few-qubit quantum computer, *Nature* **534**, 516 (2016).
- [13] W. Ji, L. Zhang, M. Wang, L. Zhang, Y. Guo, Z. Chai, X. Rong, F. Shi, X.-J. Liu, Y. Wang, *et al.*, Quantum simulation for three-dimensional chiral topological insulator, *Physical Review Letters* **125**, 020504 (2020).
- [14] P. N. Jepsen, W. W. Ho, J. Amato-Grill, I. Dimitrova, E. Demler, and W. Ketterle, Transverse spin dynamics in the anisotropic heisenberg model realized with ultracold atoms, *Physical Review X* **11**, 041054 (2021).
- [15] T. Oka and S. Kitamura, Floquet engineering of quantum materials, *Annual Review of Condensed Matter Physics* **10**, 387 (2019).
- [16] C. Schweizer, F. Grusdt, M. Berngruber, L. Barbiero, E. Demler, N. Goldman, I. Bloch, and M. Aidelsburger, Floquet approach to z_2 lattice gauge theories with ultracold atoms in optical lattices, *Nature Physics* **15**, 1168 (2019).
- [17] S. Geier, N. Thaicharoen, C. Hainaut, T. Franz, A. Salzinger, A. Tebben, D. Grimshandl, G. Zürn, and M. Weidemüller, Floquet hamiltonian engineering of an isolated many-body spin system, *Science* **374**, 1149 (2021).
- [18] F. Petiziol, S. Wimberger, A. Eckardt, and F. Mintert, Non-perturbative floquet engineering of the toric-code hamiltonian and its ground state, *arXiv preprint arXiv:2211.09724* (2022).
- [19] M. Kalinowski, N. Maskara, and M. D. Lukin, Non-abelian floquet spin liquids in a digital rydberg simulator, *Physical Review X* **13**, 031008 (2023).
- [20] H.-K. Jin, J. Knolle, and M. Knap, Fractionalized prethermalization in a driven quantum spin liquid, *Physical Review Letters* **130**, 226701 (2023).
- [21] B.-Y. Sun, N. Goldman, M. Aidelsburger, and M. Bukov, Engineering and probing non-abelian chiral spin liquids using periodically driven ultracold atoms, *PRX Quantum* **4**, 020329 (2023).
- [22] T. Kitagawa, E. Berg, M. Rudner, and E. Demler, Topological characterization of periodically driven quantum systems, *Physical Review B* **82**, 235114 (2010).
- [23] A. C. Potter, T. Morimoto, and A. Vishwanath, Classification of interacting topological floquet phases in one dimension, *Physical Review X* **6**, 041001 (2016).
- [24] P. Titum, E. Berg, M. S. Rudner, G. Refael, and N. H. Lindner, Anomalous floquet-anderson insulator as a nonadiabatic quantized charge pump, *Physical Review X* **6**, 021013 (2016).
- [25] V. Khemani, A. Lazarides, R. Moessner, and S. L. Sondhi, Phase structure of driven quantum systems, *Physical review letters* **116**, 250401 (2016).
- [26] D. V. Else, B. Bauer, and C. Nayak, Floquet time crystals, *Physical review letters* **117**, 090402 (2016).
- [27] N. Y. Yao, A. C. Potter, I.-D. Potirniche, and A. Vishwanath, Discrete time crystals: Rigidity, criticality, and realizations, *Physical review letters* **118**, 030401 (2017).
- [28] D. V. Else, W. W. Ho, and P. T. Dumitrescu, Long-lived interacting phases of matter protected by multiple time-translation symmetries in quasiperiodically driven systems, *Physical Review X* **10**, 021032 (2020).
- [29] P. T. Dumitrescu, J. G. Bohnet, J. P. Gaebler, A. Hankin, D. Hayes, A. Kumar, B. Neyenhuis, R. Vasseur, and A. C. Potter, Dynamical topological phase realized in a trapped-ion quantum simulator, *Nature* **607**, 463 (2022).
- [30] X. Zhang, W. Jiang, J. Deng, K. Wang, J. Chen, P. Zhang, W. Ren, H. Dong, S. Xu, Y. Gao, *et al.*, Digital quantum simulation of floquet symmetry-protected topological phases, *Nature* **607**, 468 (2022).
- [31] X. Mi, M. Ippoliti, C. Quintana, A. Greene, Z. Chen, J. Gross, F. Arute, K. Arya, J. Atalaya, R. Babbush, *et al.*, Time-crystalline eigenstate order on a quantum processor, *Nature* **601**, 531 (2022).
- [32] L. D’Alessio, Y. Kafri, A. Polkovnikov, and M. Rigol, From quantum chaos and eigenstate thermalization to statistical mechanics and thermodynamics, *Advances in Physics* **65**, 239 (2016).
- [33] L. Vidmar and M. Rigol, Generalized gibbs ensemble in integrable lattice models, *Journal of Statistical Mechanics: Theory and Experiment* **2016**, 064007 (2016).
- [34] C. Hainaut, I. Manai, J.-F. Clément, J. C. Garreau, P. Szriftgiser, G. Lemarié, N. Cherroret, D. Delande, and R. Chicireanu, Controlling symmetry and localization with an artificial gauge field in a disordered quantum system, *Nature communications* **9**, 1382 (2018).
- [35] A. Haldar, R. Moessner, and A. Das, Onset of floquet thermalization, *Physical Review B* **97**, 245122 (2018).
- [36] U. Agrawal, A. Zabalo, K. Chen, J. H. Wilson, A. C. Potter, J. Pixley, S. Gopalakrishnan, and R. Vasseur, Entanglement and charge-sharpening transitions in $u(1)$ symmetric monitored quantum circuits, *Physical Review X* **12**, 041002 (2022).
- [37] C. Murthy, A. Babakhani, F. Iniguez, M. Srednicki, and N. Y. Halpern, Non-abelian eigenstate thermalization hypothesis, *Physical Review Letters* **130**, 140402 (2023).
- [38] F. Kranzl, A. Lasek, M. K. Joshi, A. Kalev, R. Blatt, C. F. Roos, and N. Y. Halpern, Experimental observation of thermalization with noncommuting charges, *PRX Quantum* **4**, 020318 (2023).
- [39] D. J. Luitz, R. Moessner, S. Sondhi, and V. Khemani, Prethermalization without temperature, *Physical Review X* **10**, 021046 (2020).
- [40] W. Beatrez, C. Fleckenstein, A. Pillai, E. de Leon Sanchez, A. Akkiraju, J. Diaz Alcalá, S. Conti, P. Reshetikhin, E. Druga, M. Bukov, *et al.*,

- Critical prethermal discrete time crystal created by two-frequency driving, *Nature Physics* **19**, 407 (2023).
- [41] A. Trenkwalder, G. Spagnolli, G. Semeghini, S. Coop, M. Landini, P. Castilho, L. Pezze, G. Modugno, M. Inguscio, A. Smerzi, *et al.*, Quantum phase transitions with parity-symmetry breaking and hysteresis, *Nature physics* **12**, 826 (2016).
- [42] L. P. García-Pintos, D. Tielas, and A. Del Campo, Spontaneous symmetry breaking induced by quantum monitoring, *Physical Review Letters* **123**, 090403 (2019).
- [43] C. Kokail, C. Maier, R. van Bijnen, T. Brydges, M. K. Joshi, P. Jurcevic, C. A. Muschik, P. Silvi, R. Blatt, C. F. Roos, *et al.*, Self-verifying variational quantum simulation of lattice models, *Nature* **569**, 355 (2019).
- [44] J. Choi, H. Zhou, H. S. Knowles, R. Landig, S. Choi, and M. D. Lukin, Robust dynamic hamiltonian engineering of many-body spin systems, *Phys. Rev. X* **10**, 031002 (2020).
- [45] M. C. Tran, Y. Su, D. Carney, and J. M. Taylor, Faster digital quantum simulation by symmetry protection, *PRX Quantum* **2**, 010323 (2021).
- [46] J. Richter and A. Pal, Simulating hydrodynamics on noisy intermediate-scale quantum devices with random circuits, *Physical Review Letters* **126**, 230501 (2021).
- [47] N. Keenan, N. F. Robertson, T. Murphy, S. Zhuk, and J. Goold, Evidence of Kardar-Parisi-Zhang scaling on a digital quantum simulator, *npj Quantum Information* **9**, 72 (2023).
- [48] H. Zhao, M. Bukov, M. Heyl, and R. Moessner, Making trotterization adaptive and energy-self-correcting for nisq devices and beyond, *PRX Quantum* **4**, 030319 (2023).
- [49] H. Zhao, F. Mintert, and J. Knolle, Floquet time spirals and stable discrete-time quasicrystals in quasiperiodically driven quantum many-body systems, *Physical Review B* **100**, 134302 (2019).
- [50] B. Lapiere, K. Choo, A. Tiwari, C. Tauber, T. Neupert, and R. Chitra, Fine structure of heating in a quasiperiodically driven critical quantum system, *Physical Review Research* **2**, 033461 (2020).
- [51] X. Wen, R. Fan, A. Vishwanath, and Y. Gu, Periodically, quasiperiodically, and randomly driven conformal field theories, *Physical Review Research* **3**, 023044 (2021).
- [52] T. Mori, H. Zhao, F. Mintert, J. Knolle, and R. Moessner, Rigorous bounds on the heating rate in thue-morse quasiperiodically and randomly driven quantum many-body systems, *Physical Review Letters* **127**, 050602 (2021).
- [53] D. M. Long, P. J. Crowley, and A. Chandran, Many-body localization with quasiperiodic driving, *Physical Review B* **105**, 144204 (2022).
- [54] F. Nathan, I. Martin, and G. Refael, Topological frequency conversion in weyl semimetals, *Physical Review Research* **4**, 043060 (2022).
- [55] G. He, B. Ye, R. Gong, Z. Liu, K. W. Murch, N. Y. Yao, and C. Zu, Quasi-floquet prethermalization in a disordered dipolar spin ensemble in diamond, *Physical Review Letters* **131**, 130401 (2023).
- [56] H. Zhao, F. Mintert, R. Moessner, and J. Knolle, Random multipolar driving: Tunably slow heating through spectral engineering, *Physical Review Letters* **126**, 040601 (2021).
- [57] G. Guarnieri, M. T. Mitchison, A. Purkayastha, D. Jaksch, B. Buča, and J. Goold, Time periodicity from randomness in quantum systems, *Physical Review A* **106**, 022209 (2022).
- [58] The proof in A relies on the Baker-Campbell-Hausdorff (BCH) formula which is generalized to continuous drives via the Floquet-Magnus expansion. Since in the latter, the commutator structure decouples from the time-ordered integrals, HS can be engineered also for continuous drives.
- [59] M. Bukov, L. D'Alessio, and A. Polkovnikov, Universal high-frequency behavior of periodically driven systems: from dynamical stabilization to floquet engineering, *Advances in Physics* **64**, 139 (2015).
- [60] T. Mori, T. Kuwahara, and K. Saito, Rigorous bound on energy absorption and generic relaxation in periodically driven quantum systems, *Physical review letters* **116**, 120401 (2016).
- [61] D. A. Abanin, W. De Roeck, W. W. Ho, and F. Huveneers, Effective hamiltonians, prethermalization, and slow energy absorption in periodically driven many-body systems, *Physical Review B* **95**, 014112 (2017).
- [62] Note the difference in notation between $Q_{[M]}$ which denotes the effective IFE Hamiltonian truncated to order M , and Q_n which conserves the symmetry group G_n .
- [63] Note that there is another \mathbb{Z}_2 generated by $P_x = \prod_i \sigma_i^x$ which will not be broken by the drive. However, since this is not a subgroup of the \mathbb{Z}_2 generated by P_z , we do not consider it in the present HS example.
- [64] Such an initial state is a high-temperature state with respect to $Q_{\pm}^{(0)}$ as verified by the energy density which is close to zero.
- [65] These threshold values are chosen for numerical simplicity and the scaling exponent of the prethermal lifetime in the high-frequency regime should not depend on their specific choices.
- [66] F. M. Surace, A. Russomanno, M. Dalmonte, A. Silva, R. Fazio, and F. Jemini, Floquet time crystals in clock models, *Physical Review B* **99**, 104303 (2019).
- [67] F. Schindler, A. M. Cook, M. G. Vergniory, Z. Wang, S. S. Parkin, B. A. Bernevig, and T. Neupert, Higher-order topological insulators, *Science advances* **4**, eaat0346 (2018).
- [68] Note that, since the system is non-interacting, heating to infinite temperature does not occur even at infinite times.
- [69] J. C. Halimeh, M. Aidelsburger, F. Grusdt, P. Hauke, and B. Yang, Cold-atom quantum simulators of gauge theories, *arXiv preprint arXiv:2310.12201* (2023).
- [70] P. Faist, S. Nezami, V. V. Albert, G. Salton, F. Pastawski, P. Hayden, and J. Preskill, Continuous symmetries and approximate quantum error correction, *Physical Review X* **10**, 041018 (2020).
- [71] S. Lieu, R. Belyansky, J. T. Young, R. Lundgren, V. V. Albert, and A. V. Gorshkov, Symmetry breaking and error correction in open quantum systems, *Physical Review Letters* **125**, 240405 (2020).
- [72] G.-Y. Zhu, N. Tantivasadakarn, A. Vishwanath, S. Trebst, and R. Verresen, Nishimori's cat: stable long-range entanglement from finite-depth unitaries and weak measurements, *Physical Review Letters* **131**, 200201 (2023).
- [73] H. Sun, B. Yang, H.-Y. Wang, Z.-Y. Zhou, G.-X. Su, H.-N. Dai, Z.-S. Yuan, and J.-W. Pan, Realization of a bosonic antiferromagnet, *Nature Physics* **17**, 990 (2021).
- [74] D. Wei, A. Rubio-Abadal, B. Ye, F. Machado, J. Kemp,

- K. Srakaew, S. Hollerith, J. Rui, S. Gopalakrishnan, N. Y. Yao, *et al.*, Quantum gas microscopy of Kardar-Parisi-Zhang superdiffusion, *Science* **376**, 716 (2022).
- [75] H. Watanabe, T. Brauner, and H. Murayama, Massive Nambu-Goldstone bosons, *Physical Review Letters* **111**, 021601 (2013).
- [76] V. V. Albert and L. Jiang, Symmetries and conserved quantities in Lindblad master equations, *Physical Review A* **89**, 022118 (2014).
- [77] T. Mori, Floquet prethermalization in periodically driven classical spin systems, *Physical Review B* **98**, 104303 (2018).
- [78] T. Mori, Floquet states in open quantum systems, *Annual Review of Condensed Matter Physics* **14**, 35 (2023).
- [79] L. M. Sieberer, M. Buchhold, J. Marino, and S. Diehl, Universality in driven open quantum matter, *arXiv preprint arXiv:2312.03073* (2023).
- [80] O. Howell, P. Weinberg, D. Sels, A. Polkovnikov, and M. Bukov, Asymptotic prethermalization in periodically driven classical spin chains, *Physical Review Letters* **122**, 010602 (2019).
- [81] A. Pizzi, A. Nunnenkamp, and J. Knolle, Classical prethermal phases of matter, *Physical Review Letters* **127**, 140602 (2021).
- [82] B. Ye, F. Machado, and N. Y. Yao, Floquet phases of matter via classical prethermalization, *Physical Review Letters* **127**, 140603 (2021).
- [83] M. Yue and Z. Cai, Prethermal time-crystalline spin ice and monopole confinement in a driven magnet, *Physical Review Letters* **131**, 056502 (2023).
- [84] J. Yan, R. Moessner, and H. Zhao, Prethermalization in aperiodically kicked many-body dynamics, *arXiv preprint arXiv:2306.16144* (2023).
- [85] B. Buča and T. Prosen, A note on symmetry reductions of the Lindblad equation: transport in constrained open spin chains, *New Journal of Physics* **14**, 073007 (2012).
- [86] F. M. Surace and O. Motrunich, Weak integrability breaking perturbations of integrable models, *Phys. Rev. Res.* **5**, 043019 (2023).
- [87] T. N. Ikeda and A. Polkovnikov, Fermi's golden rule for heating in strongly driven Floquet systems, *Physical Review B* **104**, 134308 (2021).
- [88] H.-C. Yeh, A. Rosch, and A. Mitra, Decay rates of almost strong modes in Floquet spin chains beyond Fermi's golden rule, *Phys. Rev. B* **108**, 075112 (2023).

CONTENTS

A. General Protocol for Arbitrary Order of HS	11
1. General Driving Protocol: Iterative Proof	11
2. Implementing symmetry-breaking at arbitrary-order of the inverse-frequency expansion	12
3. Shortening the HS drive sequence	13
4. Generalizations of the hierarchical symmetry protocols	13
B. Fermi Golden Rule and dynamic transitions between prethermal sub-plateaux	15
1. Decay rate of Order Parameter	15
2. Decay rate of infinite-temperature auto-correlation function	17
C. Additional results on HS in spin systems	18
1. Effective Hamiltonian for $SU(2) \rightarrow U(1) \rightarrow \mathbb{Z}_2 \rightarrow E$	18
2. Effective Hamiltonian for $U(1) \rightarrow \mathbb{Z}_2 \rightarrow E$ with Floquet drives	19
3. Effective Hamiltonian for $U(1) \rightarrow \mathbb{Z}_2 \rightarrow E$ with random drives	20
D. HS in Z_4 Quantum Clock Model	21
E. High-order Topological Insulators from HS	22

Appendix A: General Protocol for Arbitrary Order of HS

1. General Driving Protocol: Iterative Proof

In this section, we prove that the recursive time-dependent construction in Eq. (3), introduced in the main text, can realize hierarchically the symmetries of the symmetry ladder

$$G_n \supset G_{n-1} \supset G_{n-2} \supset \cdots \supset G_1 \supset G_0. \quad (\text{A1})$$

We illustrate the basic idea with a simple and concrete example before discussing the general proof.

Consider a Hamiltonian H_1 which preserves the symmetry G_1 and a Hamiltonian H_0 which only preserves a subgroup G_0 of G_1 , i.e., $G_1 \supset G_0$. We construct the following Floquet operator

$$U_1 \equiv e^{-iQ_1 l_1 T} = e^{-iH_0 T} e^{-iH_1 T} e^{iH_0 T} e^{-iH_1 T}, \quad (\text{A2})$$

where $l_n \equiv -2 + 3 \times 2^n$. The effective Hamiltonian reads $Q_1 = Q_1^{(0)} + Q_1^{(1)} + \mathcal{O}(T^2)$, with $Q_1^{(0)} \sim H_1$ preserving G_1 and, $Q_1^{(1)} \sim T[H_1, H_0]$ reducing G_1 to G_0 . Notice that in Eq. (A2) the prefactors in front of the two H_0 operators differ by a sign, ensuring the exact cancellation of H_1 symmetry-reducing terms in the leading order (time-average) $Q_1^{(0)}$. This mechanism is the key ingredient for the proposed recursive construction.

Now we go one step further by introducing yet a new Hamiltonian H_2 which preserves the symmetry G_2 , such that $G_2 \supset G_1 \supset G_0$. Therefore, H_2 also preserves G_1 and G_0 by construction. The new time evolution operator is

$$U_2 \equiv e^{-iQ_2 l_2 T} = e^{-iQ_1 l_1 T} e^{-iH_2 T} e^{iQ_1 l_1 T} e^{-iH_2 T}, \quad (\text{A3})$$

where $Q_2 = Q_2^{(0)} + Q_2^{(1)} + Q_2^{(2)} + \mathcal{O}(T^3)$. Similar to the case above, the prefactors in front of Q_1 differ by a sign, and one can verify that $Q_2^{(0)} \sim H_2$ preserves G_2 , $Q_2^{(1)} \sim T[H_2, Q_1^{(0)}] \sim T[H_2, H_1]$ reduces G_2 to G_1 . Finally, $Q_2^{(2)} \sim T^2(\alpha_1[H_2, Q_1^{(1)}] + \alpha_2[H_2, [H_2, Q_1^{(0)}] + \alpha_3[Q_1^{(0)}, [Q_1^{(0)}, H_2]])$ for some coefficients α_i and, importantly, the term with prefactor α_1 reduces G_1 to G_0 since $Q_1^{(1)}$ does so alone. In general, it follows that the m -th order term $Q_2^{(m)}$ contains at most the $(m-1)$ -th order term $Q_1^{(m-1)}$ from the IFE expansion of Q_1 .

These basic observations suggest that if we iteratively construct a new evolution operator U_n , the previous HS structure can be embedded into the effective Hamiltonian of U_n , while the zeroth-order of the effective Hamiltonian is proportional to the newly added Hamiltonian which obeys the highest symmetry group. In addition, the structure of level $(n-1)$ HS ladder is embedded in the level n HS ladder. In practice, $e^{iQ_1 l_1 T}$ can be implemented by reversing the order of the temporal sequence of Eq. (A2) and conjugating each individual driving element (i.e., going backward in time).

We can now give a more general construction and its proof based on induction. Consider a set of Hamiltonian $\{H_r\}$ with a symmetry ladder $\{G_r\}$ and corresponding symmetry generators $\{S_r\}$:

$$\begin{aligned} & H_{n-1}, H_{n-2}, \dots, H_1, H_0; \\ & G_{n-1} \supset G_{n-2} \supset \dots \supset G_1 \supset G_0; \\ & [H_p, S_q] = 0, \forall q \leq p. \end{aligned} \quad (\text{A4})$$

Let us assume that the $(n-1)$ -th order time-evolution operator $U_{n-1} = e^{-iQ_{n-1}l_{n-1}T}$ has the following property

$$\begin{aligned} Q_{n-1} &= \sum_m Q_{n-1}^{(m)}, \\ [Q_{n-1}^{(m)}, S_q] &= 0, \forall q < n-m-1, \quad [Q_{n-1}^{(m)}, S_q] \neq 0, \forall q \geq n-m-1, \end{aligned} \quad (\text{A5})$$

such that U_{n-1} already implements the above level- $(n-1)$ HS.

Next we add a new Hamiltonian H_n which obeys a higher symmetry G_n ,

$$[H_n, S_n] = 0, G_n \supset G_{n-1}, \quad (\text{A6})$$

and extend the drive protocol to

$$U_n = e^{-iQ_{n-1}l_{n-1}T} e^{-iH_n T} e^{iQ_{n-1}l_{n-1}T} e^{-iH_n T} \equiv e^{-iQ_n l_n T}. \quad (\text{A7})$$

Again, the prefactors in front of two Q_{n-1} differ by a sign. One can check that, for $n=1$, we recover Eq. (A2).

Using the Baker-Campbell-Hausdorff (BCH) expansion, we get the perturbative expansion of Q_n as a power series of T

$$\begin{aligned} Q_n &= \frac{2}{l_n} H_n + \lambda_1 T [H_n, Q_{n-1}] + \lambda_2 T^2 ([H_n, [H_n, Q_{n-1}]] + l_{n-1} [Q_{n-1}, [Q_{n-1}, H_n]]) + \dots, \\ \lambda_1 &= i \frac{l_{n-1}}{l_n}, \lambda_2 = -\frac{l_{n-1}}{2l_n}. \end{aligned} \quad (\text{A8})$$

Observe that the leading order term preserves G_n ; the strength of the G_{n-1} -reducing term is renormalized by an extra factor of T ; the strength of the G_{n-2} -reducing term is renormalized by the extra factor T^2 , etc. More precisely, the $\mathcal{O}(T^m)$ term in BCH expansion of Q_n takes the following form

$$Q_n^{(m)} = \sum_{p=1}^m f_p(Q_{n-1}^{(m-p), (m-p-1), \dots, 0}), \quad (\text{A9})$$

where $f_p(Q_{n-1}^{(m-p), (m-p-1), \dots, 0})$ involves nested commutators of H_n and $Q_{n-1}^{(m-p)}, Q_{n-1}^{(m-p-1)}, \dots, Q_{n-1}^0$; for example, $f_1(Q_{n-1}^{(m-1)}) = \lambda_1 T [H_n, Q_{n-1}^{(m-1)}]$. Since the Hamiltonian with the highest order of T in $f_p(Q_{n-1}^{(m-p), (m-p-1), \dots, 0})$ is $Q_{n-1}^{(m-p)}$, which explicitly breaks the symmetry group $G_{n-1-(m-p)}$ but preserves all lower-order symmetries G_q , we have

$$[f_p(Q_{n-1}^{(m-p), \dots}), S_q] = 0, \quad \forall q < n-1-m+p. \quad (\text{A10})$$

Therefore, for $Q_n^{(m)}$, the first symmetry group along the ladder which is explicitly broken is G_{n-m} , i.e.,

$$[Q_n^{(l)}, S_q] = 0, \quad \forall q < n-m. \quad (\text{A11})$$

Note that the conditions in Eq. (A5) are now generalized to Q_n , which completes the induction step. The new symmetry ladder is Eq. (A1), as desired.

2. Implementing symmetry-breaking at arbitrary-order of the inverse-frequency expansion

The HS structure is not necessary to have the perturbations aligned order by order in the effective Hamiltonian. We can make symmetry-breaking terms appear in an arbitrarily high-order term using our proposed protocol. The proof is very intuitive: assuming that we already have the evolution operator $U_{n-1} \equiv e^{-il_{n-1}Q_{n-1}T} =$

$e^{-i\ell_{n-2}Q_{n-2}T}e^{-iH_{n-1}T}e^{i\ell_{n-2}Q_{n-2}T}e^{-iH_{n-1}T}$ with HS structure, we know that normally $Q_{n-1}^{(1)}$ breaks G_{n-1} . However, if we impose that the newly introduced Hamiltonian H_n in the protocol preserves the symmetry G_{n-1} rather than G_n , it is clear that $Q_n^{(0)}$ and $Q_n^{(1)}$ will both preserve G_{n-1} , while the G_{n-1} -breaking term will become a higher-order perturbation.

One of the simplest ways to engineer this is to choose $H_n = H_{n-1}$; the evolution operator in this case is

$$U_n \equiv e^{-i\ell_n Q_n T} = (e^{-i\ell_{n-2} Q_{n-2} T} e^{-iH_{n-1} T} e^{i\ell_{n-2} Q_{n-2} T}) e^{-iH_{n-1} T} (e^{-i\ell_{n-2} Q_{n-2} T} e^{iH_{n-1} T} e^{i\ell_{n-2} Q_{n-2} T}) e^{-iH_{n-1} T}. \quad (\text{A12})$$

Repeating this operation we can push the symmetry-breaking term to an arbitrarily high order. Moreover, this observation holds for any symmetry in the symmetry ladder.

3. Shortening the HS drive sequence

The general construction shown in Sec. A 1 is exponentially long in n . Here, we illustrate the possibility of using additional properties of the generating Hamiltonians to shorten the drive sequence. Consider the example Eq. (5) discussed in the main text

$$U_2 = (e^{-iH_0 T} e^{-iH_1 T} e^{-iH_2 T}) (e^{iH_0 T} e^{iH_1 T} e^{-iH_2 T}), \quad (\text{A13})$$

using the property $[H_0, H_1 + H_2] = 0$ we can achieve level-2 HS with a shorter driving sequence (compared to the general construction presented in Sec. A). For level-3 HS, an option for reducing the drive sequence is using U_2 above and define $U_3 = U_2 e^{-iH_3 T} U_2^\dagger e^{-iH_3 T}$ without imposing any extra limitations on H_3 , as the SU(2) case in the main text (length of the driving sequence $\ell = 14$).

Another way is to impose a condition on the structure of the newly added Hamiltonian H_3 : consider the evolution operator

$$U_3 \equiv e^{-i8Q_3 T} = (e^{-iH_0 T} e^{-iH_1 T} e^{-iH_2 T} e^{-iH_3 T}) (e^{iH_1 T} e^{iH_2 T} e^{iH_0 T} e^{-iH_3 T}). \quad (\text{A14})$$

The first three orders of Q_3 are

$$\begin{aligned} Q_3^{(0)} &\sim H_3 \\ Q_3^{(1)} &\sim iT([H_3, H_2] + [H_3 + H_2, H_1] + [H_3, H_0]) \\ Q_3^{(2)} &\sim T^2(Q_{1,2,3} + [H_0, [H_0, H_3]] - [H_3, [H_0, H_3]] + 2[H_0, ([H_1, H_2 + H_3] + [H_2, H_3])]), \end{aligned} \quad (\text{A15})$$

where $Q_{1,2,3}$ is a short-hand notation for the effective Hamiltonian that contains only commutators of H_1 , H_2 , and H_3 . In order to achieve HS structure, the terms containing H_1 and H_0 should vanish in $Q_3^{(1)}$ and terms containing H_0 should vanish in $Q_3^{(2)}$. Therefore, one of the simplest conditions one can impose is

$$[H_0, H_3] = 0, \quad [H_0, H_2] = 0, \quad [H_1, H_2 + H_3] = 0. \quad (\text{A16})$$

These special cases can be used as building blocks for longer symmetry ladders. For even higher-level HS, a driving sequence can be constructed based on the above two special cases by the previous iterative method to reduce the sequence length. Whether there exists further shortening of the pair of driving sequences with pragmatically meaningful conditions on the Hamiltonians for higher-level HS, remains an open question.

4. Generalizations of the hierarchical symmetry protocols

In this section, we will discuss two more generalizations of the protocol we proposed before, which enable us to manipulate the effective Hamiltonian in a different way. The first one generalizes the single Hamiltonian H_n to an effective Hamiltonian P_n from the symmetry-preserving driving sequence. This has important implications for the realization of HS on real quantum devices because sometimes, instead of directly simulating H_n , one may approximate its time evolution via Trotterization. One example is the 1D Heisenberg model, whose time evolution can be Trotterized into even and odd-bond updates, both of which satisfy the desired SU(2) symmetry [46]. The second one allows us to embed specific terms in the effective Hamiltonian to tailor its properties. As we will discuss in the following, we use this method to open the energy gap in the topological example, which generates a corner state.

Generalization 1. Considering the following evolution operator

$$U_n \equiv e^{-iQ_n l_n T} = e^{-iQ_{n-1} l_{n-1} T} e^{-iP_n T} e^{iQ_{n-1} l_{n-1} T} e^{-iP'_n T}, \quad (\text{A17})$$

$$e^{-iP_n T} \equiv \prod_{i=1}^{p_n} e^{-iH_{n,i} T/p_n}, \quad e^{-iP'_n T} \equiv \prod_{i=1}^{p'_n} e^{-iH'_{n,i} T/p'_n}, \quad (\text{A18})$$

where P_n and P'_n are defined as the effective Hamiltonian of the driving sequence defined in Eq. (A18) and $H_{n,i}$, $H'_{n,i}$ all preserve the symmetry G_n . The effective Hamiltonian reads

$$\begin{aligned} Q_n &= \frac{1}{\ell_n} (P_n + P'_n) + \frac{iT}{\ell_n} \left(\ell_{n-1} [P_n, Q_{n-1}] + \frac{1}{2} [P'_n, P_n] \right) \\ &\quad - \frac{T^2}{12\ell_n} (6\ell_{n-1}^2 [Q_{n-1}, [Q_{n-1}, P_n]] + 6\ell_{n-1} [P'_n, [P_n, Q_{n-1}]] + [P_n - P'_n, [P_n, P'_n]]) + \dots \end{aligned} \quad (\text{A19})$$

Similar to the proof in the previous section, we can see that for G_q -breaking perturbation, the leading order term will be $\frac{i\ell_{n-1}T}{\ell_n} [P_n^{(0)}, Q_{n-1}^{(n-q)}]$, so that the HS structure still holds.

Generalization 2. We begin with the following two evolution operators

$$\begin{aligned} U_{n-1} &\equiv e^{-i\ell_{n-1} Q_{n-1} T} = e^{-iQ_{n-2} \ell_{n-2} T} e^{-iTR_{n-1}} e^{iQ_{n-2} \ell_{n-2} T} e^{-iTR_{n-1}}, \\ U'_{n-1} &\equiv e^{-i\ell_{n-1} Q'_{n-1} T} = e^{-iQ_{n-2} T} e^{-iTR'_{n-1}} e^{iQ_{n-2} T} e^{-iTR'_{n-1}}, \end{aligned} \quad (\text{A20})$$

where R_{n-1} and R'_{n-1} are G_{n-1} -preserving effective Hamiltonians. From Generalization 1 above with $P_{n-1} = R_{n-1}$ and $P'_{n-1} = R'_{n-1}$ in Eq. (A17), it follows that both U_{n-1} and U'_{n-1} have a HS structure. Let us now consider the following evolution operator

$$U_n = U_{n-1} e^{-iTR_n} U'_{n-1} e^{-iTR_n} \equiv e^{-i\ell_n Q_n T}. \quad (\text{A21})$$

The effective Hamiltonian Q_n is

$$\begin{aligned} Q_n &= \frac{1}{\ell_n} (2R_n + \ell_{n-1} (Q_{n-1} - Q'_{n-1})) + \frac{iT}{\ell_n} \left(\ell_{n-1} [R_n, Q_{n-1}] + \frac{\ell_{n-1}^2}{2} [Q'_{n-1}, Q_{n-1}] \right) \\ &\quad - \frac{T^2}{6\ell_n} \left(\ell_{n-1}^2 [Q_{n-1}, [Q_{n-1}, R_n]] + \ell_{n-1}^2 [Q'_{n-1}, [Q'_{n-1}, R_n]] + \ell_{n-1}^2 [Q'_{n-1}, [Q_{n-1}, R_n]] \right. \\ &\quad \left. + \ell_{n-1}^2 [R_n, [Q_{n-1}, Q'_{n-1}]] + \ell_{n-1} [R_n, [R_n, 2Q_{n-1} + Q'_{n-1}]] + \frac{\ell_{n-1}^3}{2} [Q_{n-1} + Q'_{n-1}, [Q'_{n-1}, Q_{n-1}]] \right) \\ &\quad + \dots \end{aligned} \quad (\text{A22})$$

Similarly, for a G_q -breaking perturbation with $q < n$ (i.e., terms containing $Q_{n-2}^{(n-q-1)}$), the leading and subleading order term are found to be

$$\mathcal{O}(T^{n-q}): \quad \frac{\ell_{n-1}}{\ell_n} (Q_{n-1}^{(n-q)} - Q'_{n-1}^{(n-q)}) = \frac{i\ell_{n-2}T}{\ell_n} [R_{n-1}^{(0)} - R'_{n-1}^{(0)}, Q_{n-2}^{(n-q-1)}] + G_q \text{-preserving terms}, \quad (\text{A23})$$

$$\mathcal{O}(T^{n-q+1}): \quad \frac{iT}{\ell_n} \left(\ell_{n-1} [R_n, Q_{n-1}^{(n-q)}] + \frac{\ell_{n-1}^2}{2} [Q_{n-1}^{(0)}, Q_{n-1}^{(n-q)}] + \frac{\ell_{n-1}^2}{2} [Q_{n-1}^{(n-q)}, Q_{n-1}^{(0)}] \right). \quad (\text{A24})$$

Now, if we impose that $R_{n-1}^{(0)} = R'_{n-1}^{(0)}$, the leading order term in Eq. (A23) will be echoed out, and the regular $\mathcal{O}(T^{n-q+1})$ terms will be retained. For a G_n -breaking perturbation, in addition to the common term $[R_n, Q_{n-1}^{(0)}]$ we have inserted a term $Q_{n-1}^{(1)} - Q'_{n-1}^{(1)} \sim R_{n-1}^{(1)} - R'_{n-1}^{(1)}$ by means of the definition of U_n . Therefore Q_n preserves the HS structure. The inserted term consists only of G_{n-1} -preserving Hamiltonian and it may help us to achieve some specific HS. For example, in the HOTI case (c.f. Appendix E), without this generalization, we can only have $i[H_2, H_1]$ as the \mathcal{T} -breaking perturbation, which cannot open an energy gaps to get a corner state.

Appendix B: Fermi Golden Rule and dynamic transitions between prethermal sub-plateaux

The constructions presented in the last section realize a temporal sequence of HS. As shown in Fig. 2 in the main text, HS can modify significantly the thermalization pathways before the ultimate heat death. In particular, in Fig. 2 (b), we numerically show that the prethermal lifetime of the conservation laws follows the algebraic scaling T^α where $\alpha \approx 2$ and $\alpha \approx 4$, depending on the strength of the term that reduces the corresponding symmetry group. Here we justify this scaling law using a Fermi's Golden rule type argument. We first consider the dynamics of the conservation laws (or, more precisely, the order parameters) associated with the corresponding symmetry. Then we analyze the dynamics of auto-correlation functions. Both of them lead to the same scaling exponent, which matches well our numerical observations in the high-frequency regime.

1. Decay rate of Order Parameter

We first analyze the dynamics of the expectation value of the symmetry generators $S_{q,r}$ where $q \in \{n, n-1, \dots, 0\}$ associated with the relevant symmetry ladder G_q and r labels non-commuting generators of G_q . For example, in the case of $SU(2) \rightarrow U(1) \rightarrow \mathbb{Z}_2 \rightarrow E$, we have $n = 3$ and the order parameters can be chosen as $S_{3,(x,y,z)} = S_{(x,y,z)}$ for $SU(2)$ and $S_2 = S_z$ for $U(1)$; S_1 is the parity order parameter (see main text). At short times and in the high-frequency regime, the highest symmetry is approximately preserved and hence $\langle S_{n,r} \rangle$ remains almost constant in time. The system prethermalizes in the Hilbert space restricted by the highest symmetry. This soft constraint becomes less stringent at late times when the effect of the next-order perturbation, which reduces the symmetry group, becomes sizeable. Therefore, in the high-frequency limit, there should appear n -step relaxation processes, and here we want to understand the transition rate between them associated with different symmetry sectors. Technically, we follow Ref. [87] and generalize their results to cases when an approximate symmetry is present.

In the $(n-q)$ -th relaxation step, the effective Hamiltonian reads as

$$Q_{n,[n-q]} = \sum_{i=0}^{n-q} Q_n^{(i)}, \quad (\text{B1})$$

where $[n-q]$ denotes that the perturbative BCH expansion is truncated at the order $n-q$. Since $[Q_{n,[n-q]}, S_{q,r}] = 0$, there is a set of eigenstates shared by $Q_{n,[n-q]}$ and $S_{q,r}$: $\{|\ell_r\rangle\} = \{|\ell_{r,s}, \ell_{r,e}, \dots\rangle\}$. Where $\ell_{r,s}$ and $\ell_{r,e}$ are the quantum number of $S_{q,r}$ and $Q_{n,[n-q]}$ respectively (for $U(1)$ there is only one quantum number, but for $SU(2)$ there are two). The corresponding eigenvalues are given by:

$$Q_{n,[n-q]} |\ell_r\rangle = E_{q,\ell_r} |\ell_r\rangle, \quad S_{q,r} |\ell_r\rangle = N_{q,\ell_r} |\ell_r\rangle. \quad (\text{B2})$$

In a fixed prethermal plateau, the state of the system is approximately described by the generalized Gibbs ensemble [33] (for plateaus of non-Abelian symmetries, the corresponding system state is called the non-Abelian thermal state [37]). We assume that the different prethermal plateaus are well separated in time; for a fixed prethermal plateau corresponding to G_q , this timescale separation ensures that only those Lagrange multipliers that reflect the associated quasi-conservation law are taken into account. Therefore the generalized ensemble which characterizes the local properties of the system in the q -th prethermal state reads as

$$\rho_t = \frac{e^{-\beta(t)Q_{n,[n-q]} - \sum_r \mu_{q,r}(t)S_{q,r}}}{Z_t} \quad (\text{B3})$$

$$Z_t = \text{Tr}(e^{-\beta(t)Q_{n,[n-q]} - \sum_r \mu_{q,r}(t)S_{q,r}}).$$

Here $\mu_{q,r}$ and β are time-dependent Lagrange multipliers. They can be determined from the expectation values of the quasi-conserved quantities, $\langle S_{q,r} \rangle$, $\langle Q_{n,[n-q]} \rangle$ and their evolution equations are

$$\frac{d\langle S_{q,r} \rangle}{dt} = \text{Tr}(S_{q,r} \frac{d}{dt} \rho_t)$$

$$\frac{d\langle Q_{n,[n-q]} \rangle}{dt} = \text{Tr}(Q_{n,[n-q]} \frac{d}{dt} \rho_t) \quad (\text{B4})$$

However, the Lagrange multipliers β and μ_q are still undetermined. To find them we define the probability distribution function as

$$P_{\ell_r}^{\mu_q(t)} = \langle \ell_r | \rho_t | \ell_r \rangle, \langle S_{q,r} \rangle = \sum_{\ell_r} N_{q,\ell_r} P_{\ell_r}^{\mu_q(t)}, \quad (\text{B5})$$

where $\mu_q(t) = \{\beta(t), \mu_{q,0}(t), \mu_{q,1}(t), \dots\}$. We consider the master equation for $P_{\ell_r}^{\mu_q(t)}$:

$$\frac{dP_{\ell_r}^{\mu_q(t)}}{dt} = \sum_{m_r} \left(w_{m_r \rightarrow \ell_r}^{(q)} P_{m_r}^{\mu_q(t)} - w_{\ell_r \rightarrow m_r}^{(q)} P_{\ell_r}^{\mu_q(t)} \right), \quad (\text{B6})$$

where $w_{m_r \rightarrow \ell_r}^{(q)}$ is the transition rate of $S_{q,r}$ corresponding to the G_q -reducing perturbation derived from Fermi-Golden rule (FGR). Therefore we obtain a second set of evolution equations:

$$\frac{d\langle S_{q,r} \rangle}{dt} = \sum_{\ell_r} N_{q,\ell_r} \frac{dP_{\ell_r}^{\mu_q(t)}}{dt} = \sum_{\ell_r, m_r} (N_{q,\ell_r} - N_{q,m_r}) P_{m_r}^{\mu_q(t)} w_{m_r \rightarrow \ell_r}^{(q)}, \quad (\text{B7})$$

$$\frac{d\langle Q_{n,[n-q]} \rangle}{dt} = \sum_{\ell_r} E_{\ell_r} \frac{dP_{\ell_r}^{\mu_q(t)}}{dt} = \sum_{\ell_r, m_r} (E_{\ell_r} - E_{m_r}) P_{m_r}^{\mu_q(t)} w_{m_r \rightarrow \ell_r}^{(q)}. \quad (\text{B8})$$

Equations (B4) and (B7) form a set of self-consistent evolution equations for the variables $\langle S_{q,r} \rangle, \langle Q_{n,[n-q]} \rangle, \mu_{q,r}(t), \beta(t)$ describing the approximate evolution of the ensemble.

For a general time-dependent Hamiltonian $H(t) = H_n + g(t)V$, $g_f = \int_0^T \frac{dt}{T} g(t) e^{if\omega t}$ and $\omega = 2\pi/T$, the FGR transition rate is given by the expression

$$w_{m_r \rightarrow \ell_r}^{\text{FGR}} = 2\pi \sum_{f \in \mathbb{Z}} |\langle \ell_r | V | m_r \rangle_0|^2 |g_f|^2 \delta(E_{\ell_r} - E_{m_r} - f\omega), \quad (\text{B9})$$

where $|m_r\rangle_0$ and $|\ell_r\rangle_0$ are the eigenstates of H_n and $S_{q,r}$.

To obtain an estimate of the transition rates $w_{m_r \rightarrow \ell_r}^{\text{FGR}}$, we first reorganize the terms in our driving protocol in Eq. (3) by moving the right-most unitary to the right-hand side, resulting in:

$$e^{-iQ_{n-1}l_{n-1}T} e^{-iH_n T} e^{iQ_{n-1}l_{n-1}T} = e^{-iQ_n l_n T} e^{iH_n T} \equiv e^{-iQ'_{n-1}(2l_{n-1}+1)T}. \quad (\text{B10})$$

Since Q_n has a level- n HS structure and H_n preserves the highest symmetry, Q'_{n-1} also inherits the same HS structure; hence, $Q'_{n-1} = H_n T / (2l_{n-1} + 1)$. Thus the Floquet operator of our original protocol can be equivalently written as

$$U_n = e^{-iQ'_{n-1}(2l_{n-1}+1)T} e^{-iH_n T} = e^{-i(H_n + V_n)T} e^{-iH_n T}, \quad (\text{B11})$$

where $V_n = (2l_{n-1} + 1)(Q_n^{(1)} + Q_n^{(2)} + Q_n^{(3)} + \dots)$ can be regarded as the time-dependent perturbation on top of the static part H_n in the context of applying FGR.

The time-dependent function is $g(t + 2T) = g(t)$ is given by

$$g(t) = \begin{cases} 1, & \text{for } 0 < t \bmod T \leq T \\ 0, & \text{for } T < t \bmod T \leq 2T \end{cases} \quad (\text{B12})$$

Fourier transforming, we obtain $|g_f|^2 = \frac{\sin^2(fT/2)}{T^2 f^2}$. When the driving frequency $\omega = 2\pi/T$ is much larger than the norm of the local effective Hamiltonian, the system can only absorb a finite number of energy quanta (i.e., f is a finite integer). Hence in the high-frequency limit $|g_f|^2 \approx \frac{1}{4}$.

We now focus on the breaking of the symmetry G_q ($0 < q \leq n$). Note that Eq. (B7) is written in the eigenstates $|\ell_r\rangle$ and $|m_r\rangle$ of $Q_{n,[n-q]}$ and $S_{q,r}$, but the matrix element in FGR's heating rate corresponds to the eigenstates of the unperturbed Hamiltonian H_n and $S_{q,r}$. Therefore, we need to show that the matrix elements in the heating rate under these two sets of eigenbases are equal in leading order. The perturbation $Q_n^{(n-q+1)} \sim \mathcal{O}(T^{n-q+1})$ will break symmetry G_q and preserve symmetry $G_p, \forall p < q$. Since $Q_{n,[n-q]} = Q_n^{(0)} + \mathcal{O}(T) = \frac{1}{l_{n-1}+1} H_n + \mathcal{O}(T)$, it follows that $|\ell_r\rangle = |\ell_r\rangle_0 + \mathcal{O}(T)$. Therefore $\langle \ell_r | Q_n^{(n-q+1)} | m_r \rangle = \langle \ell_r | Q_n^{(n-q+1)} | m_r \rangle_0 + \mathcal{O}(T^{n-q+2})$, which means that the leading order contribution to the heating rate can be captured by the perturbed eigenstates of H_n . Now when we consider the contributions to the FGR rate we also need to take into account contributions from cross-terms in the calculation of the FGR rate $w_{m_r \rightarrow \ell_r}^{(q)} \propto |\langle \ell_r | V | m_r \rangle|^2$. However, since $[Q_n^{(n-p+1)}, S_{q,r}] = 0$ for all $q < p$ and r , the matrix element $\langle \ell_r | Q_n^{(n-p+1)} | m_r \rangle$ is nonzero only when $N_{q,\ell_r} = N_{q,m_r}$, for all $q < p$ and r . Notice that $\langle \ell_r | Q_n^{(n-q+1)} | m_r \rangle \langle m_r | Q_n^{(n-p+1)} | \ell_r \rangle$ ($q < p$) does not contribute to the heating rate associated with the order parameter $\langle S_{q,r} \rangle$ of G_q because in Eq. (B7) $N_{q,\ell_r} = N_{q,m_r}$. Therefore, the leading order contribution is

$$w_{m_r \rightarrow \ell_r}^{(q)} \sim |\langle \ell_r | Q_n^{(n-q+1)} | m_r \rangle|^2 \sim \mathcal{O}(T^{2(n-q+1)}). \quad (\text{B13})$$

2. Decay rate of infinite-temperature auto-correlation function

Here we supply another analytical approach to analyse the stability of the emergent symmetries. This is achieved by studying the time evolution of the symmetry generators $S_{n,r}(t)$, and the auto-correlation function

$$C_{n,r}(t) = \frac{1}{2L} \text{Tr}(S_{n,r}(t)S_{n,r}(0)) \quad (\text{B14})$$

at stroboscopic times $t = \ell T$ for a system of size L . If the corresponding symmetry G_n is well preserved, $C_{n,r}$ is a constant. Whereas if the symmetry is perturbed, $C_{n,r}$ generally decays and in the following, we explicitly calculate the leading order contribution to the decay rate. The result has the same scaling dependence on T as in Eq. (B13).

As we proposed, the evolution operator for n -th order HS is

$$\begin{aligned} U_n &\equiv e^{-iQ_n l_n T} = e^{-iQ_{n-1} l_{n-1} T} e^{-iH_n T} e^{iQ_{n-1} l_{n-1} T} e^{-iH_n T} \\ &= e^{-iH_n T} \left(\underbrace{e^{iH_n T} e^{-iQ_{n-1} l_{n-1} T} e^{-iH_n T} e^{iQ_{n-1} l_{n-1} T} e^{-2iH_n T}}_{U'_n} \right) e^{iH_n T}. \end{aligned} \quad (\text{B15})$$

Similarly, U'_n corresponding to Eq. (B10) also has the n -th order HS structure, which means that if we define the effective Hamiltonian Q'_n via the relation $U'_n \equiv e^{-iQ'_n l_n T}$, it will preserve G_n and break G_{n-1} . Note that, since $Q_n^{(0)} = 0$, it can be perturbatively constructed as $Q'_n = Q_n^{(1)} + Q_n^{(2)} + \dots$. We can also expand the operator U'_n accordingly as

$$U'_n = 1 - iT \left(Q_n^{(1)} + Q_n^{(2)} + \dots \right) - \frac{T^2}{2} \left(Q_n^{(1)} + Q_n^{(2)} + \dots \right) \left(Q_n^{(1)} + Q_n^{(2)} + \dots \right) + \dots \quad (\text{B16})$$

To calculate the auto-correlation function (B14), we first need to derive the time-evolved operator $S_{q,r}(T) = U_n^\dagger S_{q,r} U_n$. For simplicity, here we only consider the first two orders in the perturbation $V_1 = Q_n^{(1)}/T$ and $V_2 = Q_n^{(2)}/T^2$ and calculate the auto-correlation function of $S_{n,r}$ as an example. In the high-frequency regime, we can expand it as a power series in T

$$S_{n,r}(\ell T) \approx e^{i\mathcal{L}_n T} \left(e^{-2i\mathcal{L}_n T} \left(1 + iT^2 \mathcal{L}_{V_1} + iT^3 \mathcal{L}_{V_2} + T^4 \mathcal{G}_{V_1} + T^6 \mathcal{G}_{V_2} - \frac{T^4}{2} \mathcal{F}_{V_1} - \frac{T^6}{2} \mathcal{F}_{V_2} + T^5 \mathcal{G}_{V_{1,2}} - \frac{T^5}{2} \mathcal{F}_{V_{1,2}} \right) \right)^\ell S_{n,r}(0), \quad (\text{B17})$$

where $\mathcal{L}_n S_{n,r} = [H_n, S_{n,r}]$, $\mathcal{L}_{V_i} S_{n,r} = [V_i, S_{n,r}]$, $\mathcal{G}_{V_i} S_{n,r} = V_i S_{n,r} V_i$, $\mathcal{F}_{V_i} S_{n,r} = \{V_i^2, S_{n,r}\}$, $\mathcal{G}_{V_{i,j}} S_{n,r} = V_i S_{n,r} V_j + V_j S_{n,r} V_i$, $\mathcal{F}_{V_{i,j}} S_{n,r} = \{\{V_i, V_j\}, S_{n,r}\}$ with $\{\cdot, \cdot\}$ the anticommutator, and the perturbation $V_p = Q_n^{(p)}/T^p$ which is indeed T -independent. We also used the property that H_n preserves all the symmetries in the symmetry ladder, i.e., $e^{iH_n T} S_{q,r} e^{-iH_n T} = S_{q,r}$ for $0 \leq q \leq n$ and $\forall r$, to derive the equation above.

We insert Eq. (B17) into the definition of the autocorrelation function in Eq. (B14). Using the properties [88]

$$\begin{aligned} \text{Tr} \left(e^{-i\mathcal{L}_V T} \hat{A} \hat{B} \right) &= \text{Tr} \left(\hat{A} e^{i\mathcal{L}_V T} \hat{B} \right), \\ \text{Tr} \left(e^{-2i\mathcal{L}_n T l} (i\mathcal{L}_{V_j}) e^{-2i\mathcal{L}_n T m} S_{n,r} S_{n,r} \right) &= 0, \quad \forall j, l, m, \end{aligned} \quad (\text{B18})$$

we can get the first three orders of the T -expansion for $C_{n,r} = C_{n,r}^{(0)} + C_{n,r}^{(1)} + C_{n,r}^{(2)} + \dots$, as:

$$\begin{aligned} C_{n,r}^{(0)} &= \frac{1}{2L} \text{Tr} \left(e^{-2\ell T i \mathcal{L}_n} S_{n,r} S_{n,r} \right) = 1, \\ C_{n,r}^{(1)} &= \frac{T^4}{2L} \left(\sum_{l \geq 1, m \geq 0}^{l+m=\ell-1} \text{Tr} \left(e^{-2i\mathcal{L}_n T(\ell-m-l)} (i\mathcal{L}_{V_1}) e^{-2i\mathcal{L}_n T l} (i\mathcal{L}_{V_1}) e^{-2i\mathcal{L}_n T m} S_{n,r} S_{n,r} \right) + \sum_{l=0}^{\ell-1} \text{Tr} \left(e^{-2i\mathcal{L}_n T(\ell-l)} \mathcal{G}_{V_1} e^{-2i\mathcal{L}_n T l} S_{n,r} S_{n,r} \right) \right. \\ &\quad \left. + \sum_{l=0}^{\ell-1} \text{Tr} \left(e^{-2i\mathcal{L}_n T(\ell-l)} \left(-\frac{1}{2} \mathcal{F}_{V_1} \right) e^{-2i\mathcal{L}_n T l} S_{n,r} S_{n,r} \right) \right), \\ C_{n,r}^{(2)} &= \frac{T^5}{2L} \left(\sum_{l \geq 1, m \geq 0}^{l+m=\ell-1} \text{Tr} \left(e^{-2i\mathcal{L}_n T(\ell-l-m)} (i\mathcal{L}_{V_1} e^{-2i\mathcal{L}_n T l} i\mathcal{L}_{V_2} + i\mathcal{L}_{V_2} e^{-2i\mathcal{L}_n T l} i\mathcal{L}_{V_1}) e^{-2i\mathcal{L}_n T m} S_{n,r} S_{n,r} \right) \right. \\ &\quad \left. + \sum_{l=0}^{\ell-1} \text{Tr} \left(e^{-2i\mathcal{L}_n T(\ell-l)} \mathcal{G}_{V_{1,2}} e^{-2i\mathcal{L}_n T l} S_{n,r} S_{n,r} \right) + \text{Tr} \left(e^{-2i\mathcal{L}_n T(\ell-l)} \left(-\frac{1}{2} \mathcal{F}_{V_{1,2}} \right) e^{-2i\mathcal{L}_n T l} S_{n,r} S_{n,r} \right) \right). \end{aligned} \quad (\text{B19})$$

In fact $C_{n,r}^{(1)}$ can be simplified as

$$\begin{aligned}
C_{n,r}^{(1)} &= \frac{\ell T^4}{2L} \left(\sum_{l=1}^{\ell-1} \left(1 - \frac{l}{\ell}\right) \text{Tr} \left(e^{-2i\mathcal{L}_n T l} (i\mathcal{L}_{V_1} S_{n,r}) (-i\mathcal{L}_{V_1} S_{n,r}) \right) + \text{Tr} (V_1 S_{n,r} V_1 S_{n,r}) - \frac{1}{2} \text{Tr} (\{V_1^2, S_{n,r}\} S_{n,r}) \right) \\
&\xrightarrow{\ell \rightarrow \infty} -\frac{\ell T^4}{2L} \left(\frac{1}{2} \text{Tr} (\dot{S}_{n,r} \dot{S}_{n,r}) + \sum_{l=1}^{\infty} \text{Tr} \left(e^{-2i\mathcal{L}_n T l} \dot{S}_{n,r} \dot{S}_{n,r} \right) \right) \\
&= -\frac{\ell T^4}{2L} \sum_{i,j} \left(\frac{1}{2} + \sum_{\ell=1}^{\infty} e^{-2i\ell T(\epsilon_i - \epsilon_j)} \right) |\langle i | \dot{S}_{n,r} | j \rangle|^2 \\
&= -\frac{\ell T^3}{2L} \sum_{i,j} |\langle i | \dot{S}_{n,r} | j \rangle|^2 \frac{\pi}{2} \delta_F(\epsilon_i - \epsilon_j), \tag{B20}
\end{aligned}$$

where we use $H_n |i\rangle = \epsilon_i |i\rangle$, $\dot{S}_{n,r} \equiv i\mathcal{L}_{V_1} S_{n,r}$, $\delta_F(\epsilon_i - \epsilon_j) = \sum_{p=-\infty}^{\infty} \delta(\epsilon_i - \epsilon_j + \frac{p\pi}{T})$ and

$$\frac{1}{2} + \sum_{\ell=1}^{\infty} e^{-2i\ell T(\epsilon_i - \epsilon_j)} = \frac{1}{2} \sum_{\ell=-\infty}^{\infty} e^{-2i\ell T(\epsilon_i - \epsilon_j)} = \sum_{p=-\infty}^{\infty} \pi \delta(2T(\epsilon_i - \epsilon_j) + 2p\pi) = \frac{\pi}{2T} \sum_{p=-\infty}^{\infty} \delta(\epsilon_i - \epsilon_j + \frac{p\pi}{T}). \tag{B21}$$

Since usually the correlation function $\text{Tr} (e^{-2i\mathcal{L}_n T l} (i\mathcal{L}_{V_1} S_{n,r}) (-i\mathcal{L}_{V_1} S_{n,r}))$ decays rapidly as l increases, here $(1 - l/\ell)$ in the summation $\sum_{l=1}^{\ell-1}$ in (B20) can be approximated as 1 as $\ell \rightarrow \infty$. We can also do a similar simplification to the $C_{n,r}^{(2)}$.

Assuming $C_{n,r}(\ell T) = e^{-\Gamma_{n,r} \ell T} \approx 1 - \Gamma_{n,r} \ell T$, the heating rate $\Gamma_{n,r}$ is given by

$$\begin{aligned}
\Gamma_{n,r} &= \frac{T^2}{2L} \sum_{i,j} |\langle i | \mathcal{L}_{V_1} S_{n,r} | j \rangle|^2 \frac{\pi}{2} \delta_F(\epsilon_i - \epsilon_j) + \frac{T^3}{2L} \sum_{i,j} \frac{1}{2} (\langle i | \mathcal{L}_{V_1} S_{n,r} | j \rangle \langle j | \mathcal{L}_{V_2} S_{n,r} | i \rangle \\
&\quad + \langle i | \mathcal{L}_{V_2} S_{n,r} | j \rangle \langle j | \mathcal{L}_{V_1} S_{n,r} | i \rangle) \frac{\pi}{2} \delta_F(\epsilon_i - \epsilon_j) + \mathcal{O}(T^4). \tag{B22}
\end{aligned}$$

The first and second terms correspond to the leading order and a cross term in the FGR results of the previous section, respectively.

When the auto-correlation function of $S_{n-1,r'}$ (i.e., the second plateau) is considered, we see that the first term and second term (the cross term corresponding to $C_{n,r}^{(2)}$) in Eq. (B22) vanishes since V_1 preserves the symmetry G_{n-1} . Similarly, for a general symmetry generator $S_{q,r}$ with $1 \leq q \leq n$ and $\forall r, [S_{q,r}, V_i] = 0$ for $i \leq n - q$, it follows that any combination of terms containing \mathcal{L}_{V_i} in the expansion of $\Gamma_{q,r}$ vanish. The leading order in the decay rate $\Gamma_{q,r}$ is then

$$\Gamma_{q,r} = \frac{T^{2(n-q+1)}}{2L} \sum_{i,j} |\langle i | \mathcal{L}_{V_{n-q+1}} S_{q,r} | j \rangle|^2 + \mathcal{O}(T^{2n-2q+3}). \tag{B23}$$

This gives the same prethermal time scale $\tau_q \sim \mathcal{O}(T^{-2(n-q+1)})$, as in the former section, cf. Eq. (B13).

Appendix C: Additional results on HS in spin systems

In this section, we first show the concrete form of the effective Hamiltonians for $SU(2) \rightarrow U(1) \rightarrow \mathbb{Z}_2 \rightarrow E$ in spin systems. We also present the results of the lower order HS symmetry ladder (i.e., $U(1) \rightarrow \mathbb{Z}_2 \rightarrow E$) under the Floquet and random drives, where we introduce the participation entropy to show the distribution of the state population in different magnetization blocks. For randomly driven cases, we show numerically the decay of parity and illustrate that the \mathbb{Z}_2 -plateau is also parametrically long lived by increasing the driving frequency.

1. Effective Hamiltonian for $SU(2) \rightarrow U(1) \rightarrow \mathbb{Z}_2 \rightarrow E$

In the main text, we construct four kick generators (Eq. (7)) preserving each symmetry in the symmetry ladder $SU(2) \rightarrow U(1) \rightarrow \mathbb{Z}_2 \rightarrow E$. With the evolution operator defined in Eq. (6), the first three orders of the effective

Hamiltonian are

$$\begin{aligned}
Q^{(0)} &= \frac{1}{7}H_3, \quad Q^{(1)} = -\frac{iT}{98}[H_2, H_3], \\
Q^{(2)} &= \frac{T^2}{2184}([H_3, [H_1, H_2]] - \frac{1}{2}[H_3, [H_3, H_2]] - [H_2, [H_2, H_3]]), \\
Q_{\pm}^{(3)} &= \text{terms containing } H_0^{\pm},
\end{aligned} \tag{C1}$$

where $Q^{(0)}$ preserves the highest symmetry $SU(2)$, $Q^{(1)}$ reduces $SU(2)$ to $U(1)$, $Q^{(2)}$ reduces $U(1)$ to \mathbb{Z}_2 and higher-order terms break all symmetries.

2. Effective Hamiltonian for $U(1) \rightarrow \mathbb{Z}_2 \rightarrow E$ with Floquet drives

In the main text, we also briefly mention the sequences $U(1) \rightarrow \mathbb{Z}_2 \rightarrow E$. This level-2 HS ladder can be realized in spin systems using a Floquet drive. The kick generators are chosen as

$$H_2 = J \sum_{\langle i,j \rangle} \sigma_i^x \sigma_j^x + \sigma_i^y \sigma_j^y - \sigma_i^z \sigma_j^z, \quad H_1 = -J \sum_{\langle i,j \rangle} \sigma_i^y \sigma_j^y - \sigma_i^z \sigma_j^z, \quad H_0 = -\delta_x \sum_i \sigma_i^x, \tag{C2}$$

where the zz -interaction is added to make the model non-integrable. Each generator preserves one symmetry in the symmetry ladder. To achieve a HS structure, the time evolution operator is defined as

$$U_F = U\left(-H_0, H_1, H_2 \middle| \frac{T}{6}\right) U\left(H_0, -H_1, H_2 \middle| \frac{T}{6}\right), \tag{C3}$$

where again we use $U(D_1, \dots, D_l | T) = e^{-iD_1 T} \dots e^{-iD_l T}$. Using the property $[H_0, H_1 + H_2] = 0$, the leading three orders of effective Hamiltonian read

$$Q^{(0)} = \frac{1}{3}H_2, \quad Q^{(1)} = -\frac{iT}{36}[H_1, H_2], \quad Q^{(2)} = -\frac{T^2}{432}[H_0 + H_1 - H_2, [H_1, H_2]]. \tag{C4}$$

The zeroth order of effective Hamiltonian $Q^{(0)}$ preserves the highest symmetry $U(1)$, the first order term $Q^{(1)}$ reduces $U(1)$ to \mathbb{Z}_2 , while second-order term $Q^{(2)}$ breaks explicitly the \mathbb{Z}_2 symmetry. Therefore we expect the state of the system to go through two prethermal plateaus – for the $U(1)$ and \mathbb{Z}_2 symmetry, characterized by the z -magnetization and the parity [see main text], respectively.

We perform numerical simulations for a system size of $L = 14$ spins. The initial state is a Haar-random state in the magnetization block containing $N_{\downarrow} = 4$ down spins. We compute the energy density $\overline{E} = \langle Q^{(0)} \rangle / L$ and the magnetization density along z -axis $\overline{S}_z = \langle \sum_i \sigma_i^z \rangle / L$, where the overline means the average over different realizations of the initial state. To investigate the distribution of the evolved state in different magnetization blocks, we also compute the participation entropy [39]

$$S_{\text{part}}[\psi, N_{\downarrow}] = - \sum_{|i\rangle \in \mathcal{H}|_{N_{\downarrow}}} |\langle i|\psi\rangle|^2 \ln(|\langle i|\psi\rangle|^2). \tag{C5}$$

If the state of the system is only in a certain magnetization sector, its participation entropy on the other sector is 0. And for the thermal state, $S_{\text{part}}[\psi, N_{\downarrow}] = \dim(\mathcal{H}|_{N_{\downarrow}}) L \ln 2 / 2^L$, where L is the system size. As shown in Fig. 5(a), energy of the system is sufficiently close to zero, suggesting that the initial state corresponds to a very high temperature. Different colors correspond to different driving frequencies, and for all cases the energy density remains approximately the same as its initial value. We do not see notable changes in energy throughout the entire time evolution. It occurs possibly because the system size is not large enough and the driving frequency may be already comparable or even larger than the many-body band width, hence heating is significantly suppressed.

In contrast, dynamics of magnetization \overline{S}_z is more sensitive to the variation of the driving frequency. In Fig. 5(b), the density of magnetization decays after the first $U(1)$ prethermal plateau since the first-order effective Hamiltonian reduces $U(1)$ to \mathbb{Z}_2 . To see the effect of the approximated \mathbb{Z}_2 symmetry, we further analyse the participation entropy shown in Fig. 5(c) and (d). After the initial transient period, we see that the participation entropy for the even magnetization sectors grows notably, verifying the existence of the remaining \mathbb{Z}_2 symmetry. However, participation entropy does not evolve to its infinite temperature value (dashed lines), suggesting that the \mathbb{Z}_2 symmetry does not appear to be strongly broken by the Floquet drive. We attribute this to finite-size effects.

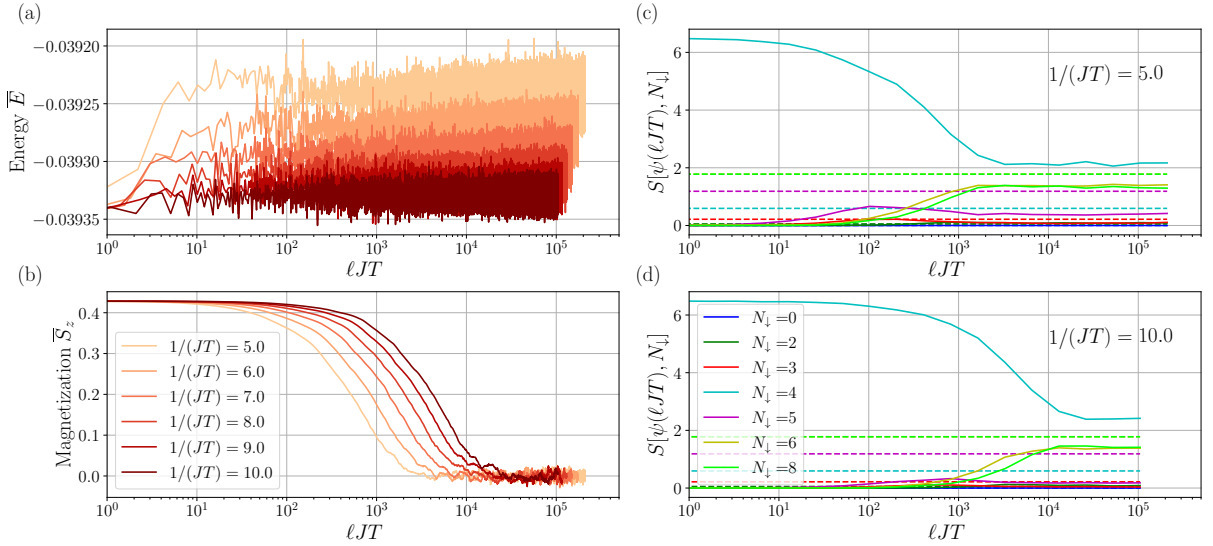


FIG. 5. Dynamical detection of $U(1) \rightarrow \mathbb{Z}_2$ HS with Floquet drives. (a) Time evolution of the density of energy $\bar{E} = \overline{\langle Q^{(0)} \rangle} / L$. We show the energy prethermal plateau where energy is quasi-conserved. However, for a small system, it is difficult to fully thermalize under the Floquet drive even at long times due to finite-size effects. (b) Dynamics of the density of magnetization $\bar{S}_z = \overline{\langle \sum_i \sigma_i^z \rangle} / L$. The lifetime of $U(1)$ plateau is prolonged with increasing driving frequency. (c),(d) The time evolution of the participation entropy for $1/(JT) = 5.0, 10.0$. N_\downarrow represents number of downwards spins. The state has weight mainly in the even magnetization sector, showing the \mathbb{Z}_2 plateau. Dashed lines represent participation entropy at infinite temperature. The parameters are $L = 14$ with symmetry-breaking perturbation strength $\delta_x/J = 10.0$. The numerical simulations are performed using exact diagonalization and 20 random realizations are used to compute the ensemble average over different initial states.

In Fig. 5(c,d), we also note that the $N_\downarrow = 5$ (but also other odd-valued) magnetization sector acquires a finite population at intermediate times. This is because the sub-leading order in the heating rate, which contains the \mathbb{Z}_2 symmetry breaking term, affects the dynamics of the system for a sufficiently long time at small driving frequencies. However, the peak will be suppressed as the driving frequency increases.

3. Effective Hamiltonian for $U(1) \rightarrow \mathbb{Z}_2 \rightarrow E$ with random drives

Finite size effect becomes less notable if we switch to random drives. We still use the same kick generators ($H_{2,1}$) as defined above in the Floquet case. However, the \mathbb{Z}_2 breaking term can occur randomly in time. More concretely, we consider

$$H_0^\pm = (\delta_x \pm \epsilon) \sum_i \sigma_i^x. \quad (C6)$$

and the evolution operator is redefined as

$$U_\pm = U \left(-H_0^\pm, H_1, H_2 \middle| \frac{T}{6} \right) U \left(H_0^\pm, -H_1, H_2 \middle| \frac{T}{6} \right). \quad (C7)$$

The U_\pm are then randomly aligned to form a stochastic drive sequence. Similar to the discussion in the Floquet case, the effective Hamiltonian Q_\pm of the evolution operator U_\pm has the same HS structure; in particular, we have $Q_-^{(0),(1)} = Q_+^{(0),(1)}$, but the randomness affects the \mathbb{Z}_2 plateau since $Q_-^{(2)} \neq Q_+^{(2)}$.

Once again, we perform a numerical simulation for a system of $L = 14$ spins, starting from a Haar-random initial state within the z -magnetization sector $N_\downarrow = 4$; this is a high-temperature (i.e., energy density) state. In Fig. 6(a1) and (a2), the system shows two clear prethermal plateaus corresponding to the $U(1)$ and \mathbb{Z}_2 symmetries. We can clearly see the HS is well achieved dynamically through our protocol. In Fig. 6(c1) and (c2), we also show the \mathbb{Z}_2 plateau exhibited by the participation entropy, during which the state is mainly distributed over the even magnetization sectors. At infinite times, the system will eventually fully thermalize, as indicated by the data in Fig. 6(c1), and the curve of participation entropy will reach the dashed line corresponding to a fully thermalized state. Note that at small driving frequencies, the \mathbb{Z}_2 symmetry breaking already kicks in at early times, but this effect can be pushed

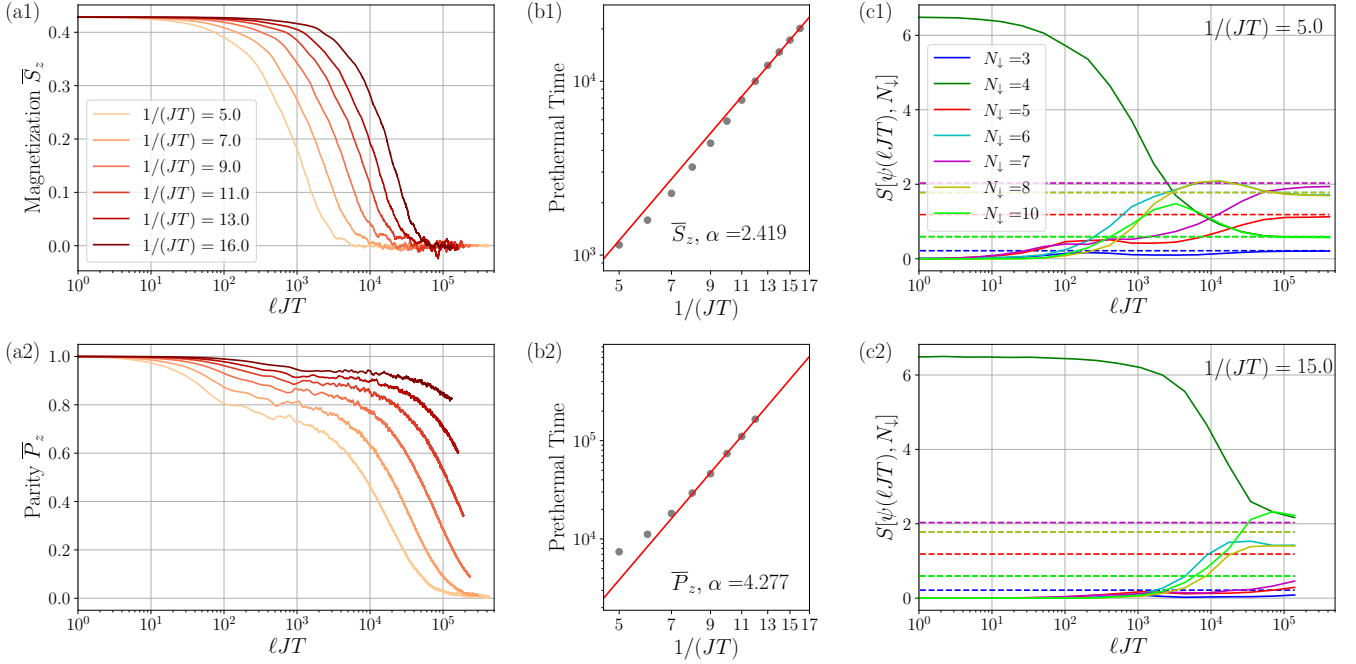


FIG. 6. Dynamical detection of $U(1) \rightarrow \mathbb{Z}_2 \rightarrow E$ HS with RMD. (a1) The time evolution of magnetization density $\overline{S}_z = \langle \sum_i \sigma_i^z \rangle / L$. The quasi-conserved magnetization shows the $U(1)$ plateau. (a2) The time evolution of the expectation value of the parity $\overline{P}_z = \langle \prod_i \sigma_i^z \rangle$. The quasi-conserved parity shows the \mathbb{Z}_2 plateau. The breaking of early conservation is suppressed with increasing drive frequency. (b1),(b2) The scaling of the prethermal lifetime of the $U(1)$ plateau and the \mathbb{Z}_2 plateau $\tau_m \sim T^{-2.419}$, $\tau_p \sim T^{-4.277}$ respectively, shows that the lifetime of HS can be dynamically prolonged by increasing the drive frequency. (c1),(c2) The time evolution of the participation entropy at drive frequencies $1/JT = 5.0$ and $1/JT = 15.0$, showing the distribution of state in each block. The Dashed lines represent the corresponding participation entropies at infinite temperature. The curves at low drive frequencies eventually coincide with the dashed lines, indicating that the system effectively heats up to an infinite-temperature state. The system size $L = 14$, the symmetry-breaking perturbations are $\delta_x/J = 10.0$, $\epsilon/J = 6.0$. The numerical simulations are performed using exact diagonalization and 20 random realizations of the driving protocol and initial state are used to compute the ensemble average. The difference in simulation results between different realizations is very small, so we don't need too many realizations.

to parametrically longer times with increasing drive frequency. We define the lifetimes τ_m and τ_p as the time for \overline{S}_z and \overline{P}_z to decay to e^{-1} of their initial values in Fig. 6(a1) and (a2). In Fig. 6(b1) and (b2), we numerically show that the time scaling of the lifetimes τ_m and τ_p are approximately $\tau_m \sim T^{-2.419}$, $\tau_p \sim T^{-4.255}$. The lifetime of the $U(1)$ plateau approximately agrees well with the FGR scaling T^{-2} . The observed deviation is mainly due to the drive frequency not being large enough, where the \mathbb{Z}_2 -breaking term is of comparable absolute magnitude to the leading order term \mathbb{Z}_2 -preserving term (cf. Sec. B); thus, the next leading-order term will affect the dynamics during the $U(1)$ plateau, which can be observed in the early-time dynamics of both the parity operator and the participation entropy. We emphasize that since the parity operator is a non-local operator, its dynamics may not be described by FGR. However, the numerical data clearly shows that the \mathbb{Z}_2 -plateau lifetime can be parametrically controlled by modulating the drive frequency.

Appendix D: HS in \mathbb{Z}_4 Quantum Clock Model

In this section, we give the details of the effective Hamiltonian corresponding to the HS ladder that implements the \mathbb{Z}_4 quantum clock model. Consider the two Hamiltonians H_1 and H_0 that preserve the \mathbb{Z}_4 and \mathbb{Z}_2 symmetry,

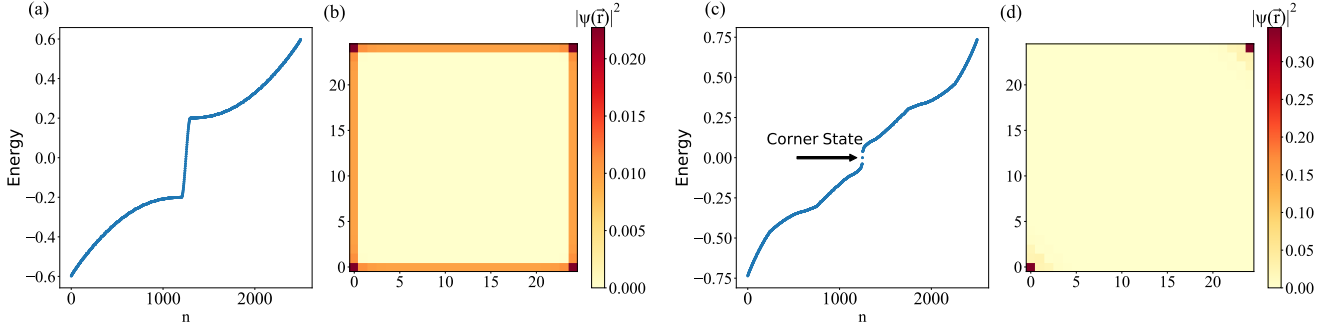


FIG. 7. Energy spectrum and zero energy state of TI and HOTI. (a),(c) Energy spectrum of $Q^{(0)}$ and $Q^{(0)} + Q^{(1)}$ respectively. (b),(d) Density distribution corresponding to the zero energy mode of $Q^{(0)}$ and $Q^{(0)} + Q^{(1)}$ respectively (e.g., edge state and corner state). The parameters are $M = 1.0, t = 1.0, \Delta_0 = 1.0, \Delta_1 = 7.0$, system size is $L = 19$.

respectively:

$$\begin{aligned}
 H_1 &= \sum_{\langle i,j \rangle} J_{ij} \left(Z_i^2 Z_j^2 - \eta (e^{i\phi} Z_i^\dagger Z_j + \text{h.c.}) \right) + \sum_i h_i \left(Z_i^2 - \frac{1}{2} (X_i + X_i^\dagger) \right) + \sum_i g_i X_i^2, \\
 H_0 &= \sum_{i=1}^L b_i (Z_i + Z_i^\dagger).
 \end{aligned} \tag{D1}$$

Following the driving protocol defined in Sec. III B, the effective Hamiltonian over four drive periods, $U_F^4 = e^{-iQ_4 T}$, is:

$$\begin{aligned}
 Q &= Q^{(0)} + Q^{(1)} + Q^{(2)} + \mathcal{O}(T^3), \\
 Q^{(0)} &= \frac{1}{2} \sum_{\langle i,j \rangle} J_{ij} \left(Z_i^2 Z_j^2 - \eta (e^{i\phi} Z_i^\dagger Z_j + e^{-i\phi} Z_i Z_j^\dagger) \right) + \frac{1}{2} \sum_i g_i X_i^2 - \frac{1}{2} \sum_i h_i (X_i + X_i^\dagger), \\
 Q^{(1)} &= \frac{iT}{16} \sum_i h_i^2 [Z_i^2, X_i + X_i^\dagger], \\
 Q^{(2)} &= \frac{T^2}{128} \left([Q^{(0)}, [Q^{(0)}, \sum_l b_l ((2-i)Z_l + (2+i)Z_l^\dagger)]] + \frac{1}{2} [\sum_l h_l Z_l^2, [Q^{(0)}, \sum_m b_m ((1-i)Z_m + (1+i)Z_m^\dagger)]] \right).
 \end{aligned} \tag{D2}$$

A Hamiltonian \mathcal{O} is Z_4 and Z_2 -preserving when $[\mathcal{O}, \prod_i X_i] = 0$ and $[\mathcal{O}, \prod_i X_i^2] = 0$. Clearly $[Q^{(0)}, \prod_i X_i] = 0$; $[Q^{(1)}, \prod_i X_i] \neq 0$, $[Q^{(1)}, \prod_i X_i^2] = 0$; $[Q^{(2)}, \prod_i X_i] \neq 0$, $[Q^{(2)}, \prod_i X_i^2] \neq 0$, showing the $Z_4 \rightarrow Z_2 \rightarrow E$ HS.

Appendix E: High-order Topological Insulators from HS

In this section, we elaborate on the HS setup implementing a change of topology from a TI to a HOTI. We give explicit expressions for the representation of the generating Hamiltonians in real space proposed in the main text for a possible experimental realization.

$$\begin{aligned}
 H_2 &= \frac{M}{2} \sum_{\vec{r}, \alpha=0,1} (-1)^\alpha c_{\vec{r}, \alpha}^\dagger c_{\vec{r}, \alpha} + \sum_{\vec{r}, \alpha=0,1} \sum_{j=x,y} \left(\frac{J}{2} (-1)^\alpha c_{\vec{r}+\vec{e}_j, \alpha}^\dagger c_{\vec{r}, \alpha} + \frac{\Delta_0}{2i} c_{\vec{r}+\vec{e}_j, \alpha+1}^\dagger \sigma_j c_{\vec{r}, \alpha} \right) + \text{h.c.}, \\
 H_1 &= \Delta_1 \sum_{\vec{r}, \alpha=0,1} (-1)^\alpha c_{\vec{r}, \alpha}^\dagger (\sigma_x + \sigma_y) c_{\vec{r}, \alpha}, \\
 H'_1 &= \Delta_1 \sum_{\vec{r}, \alpha=0,1} (-1)^\alpha c_{\vec{r}, \alpha}^\dagger \sigma_z c_{\vec{r}, \alpha}, \\
 H_0 &= \Delta_2 \sum_{\vec{r}, \alpha=0,1} c_{\vec{r}, \alpha+1}^\dagger \sigma_y c_{\vec{r}, \alpha},
 \end{aligned} \tag{E1}$$

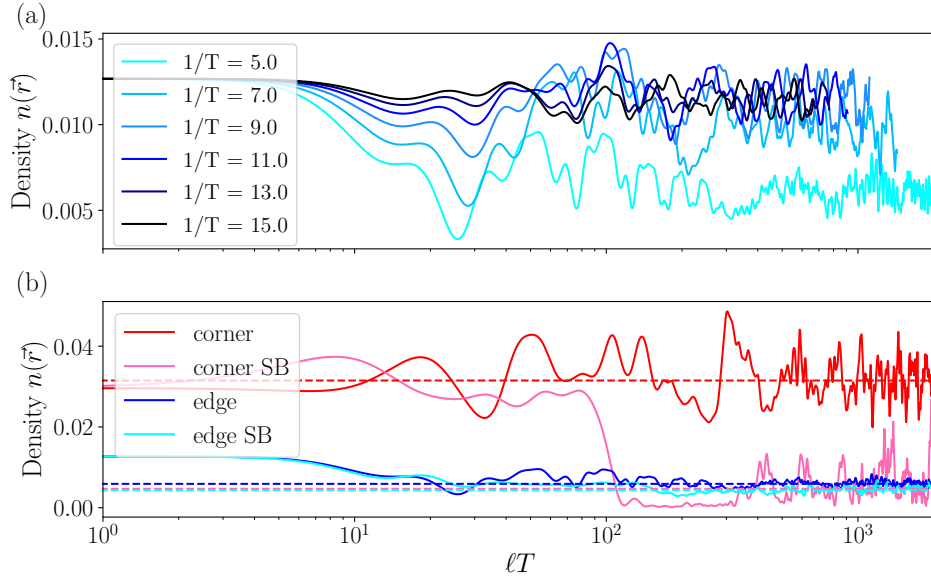


FIG. 8. HOTT results when the initial state is the zero-energy eigenstate of $Q^{(0)}$ (i.e., edge state). (a) Time evolution of the electron density at corner and edge ($n_{\text{corner}} = (n(0,0) + n(L,L))/2$, $n_{\text{edge}} = 2 \sum_{i=L/4}^{3L/4} n(i,0)/L$) without \mathcal{I} -breaking perturbation in $Q^{(1)}$ (marked by 'corner' and 'edge' labels in legend) and with \mathcal{I} -breaking perturbation ('corner SB' and 'edge SB' labels). When \mathcal{I} is preserved in the first order effective Hamiltonian, density distribution at corners has a longer lifetime showing the existence of corner state. (b) Time evolution of electron density at the edge without \mathcal{I} -breaking perturbation for different drive frequency $1/T$. The lifetime of the boundary state (i.e., the first plateau) is significantly prolonged with increasing driving frequency. The system size is $L = 19$ and the parameters are $M/J = 1.0$, $\Delta_0/J = 1.0$, $\Delta_1/J = 7.0$, and $\Delta_2/J = 12.0$.

where $c_{\vec{r},\alpha} = (c_{\vec{r},\alpha,\uparrow}, c_{\vec{r},\alpha,\downarrow})$. We can also convert the fermionic orbital as well as the spin degrees of freedom equivalently into four sites in each unit cell $(c_{\vec{r},0,\uparrow}, c_{\vec{r},0,\downarrow}, c_{\vec{r},1,\uparrow}, c_{\vec{r},1,\downarrow}) \rightarrow (c_{\vec{r},0}, c_{\vec{r},1}, c_{\vec{r},2}, c_{\vec{r},3})$. The protocol is thus also possibly realizable in ultra-cold atomic systems.

With the evolution operator defined in Eq. (11), the effective Hamiltonian $U_F \equiv e^{-iQT}$ is

$$Q = Q^{(0)} + Q^{(1)} + \mathcal{O}(T^2), \quad Q^{(0)} = \frac{1}{5}H_2, \quad Q^{(1)} = -\frac{iT}{200}([H_1, H'_1] + 2[H_1 + H'_1, H_2]). \quad (\text{E2})$$

$Q^{(0)} \propto H_2$ is a standard Hamiltonian for a TI. As what we discuss in Sec. A 4, the commutator of H_1 and H'_1 in $Q^{(1)}$ introduces an on-site \mathcal{T} -breaking but \mathcal{I} -preserving perturbation which opens the energy gap and leaves two degenerate zero-energy corner states. In Fig. 7 we present the energy spectrum and the density distribution of the zero-energy eigenstates of $Q^{(0)}$ and $Q^{(0)} + Q^{(1)}$, respectively. We can clearly see the boundary states that characterize these two topological states of matter.

In the main text, we initialize the system as a product state with a large spatial support on the edge. Such a state can be experimentally prepared, for instance, by using cold atoms in optical lattices. We expect to observe a plateau of the particle density around the edge, which should be more pronounced by increasing the driving frequency, such that $Q^{(0)}$ dominates the early time evolution. However, technically, it is difficult to show a clear plateau because this product state can delocalize quickly into the bulk, and the remaining population around the edge is comparably weak, even in the absence of the first-order perturbation $Q^{(1)}$. To confirm the existence of this plateau, here we supply numerical simulation of the dynamics by starting from the zero-energy eigenstate of $Q^{(0)}$ (i.e., the edge states), such that only higher-order perturbations delocalizes the system. As shown in Fig. 8(a), as we increase the drive frequency, the decay of the electron density at the boundary slows down accordingly, revealing the first plateau of $Q^{(0)}$. In Fig. 8(b), we show the time evolution of the electron density at the corners and boundaries with and without an \mathcal{I} -breaking perturbation. In the presence of the perturbation, labeled by 'corner SB' and 'edge SB', the density distribution on the corners decays quickly and agrees with the density distribution on the edges at long times. However, without the \mathcal{I} -breaking perturbation, the lifetime of the density distribution at the corners is visibly prolonged by an order of magnitude.